*J. Fluid Mech.* (2000), *vol.* 424, *pp.* 243–277. Printed in the United Kingdom



# Static wall layers in the displacement of two visco-plastic fluids in a plane channel

By M. ALLOUCHE[1], I. A. FRIGAARD[2,3]† AND G. SONA[4]

[1]Schlumberger Dowell, 26 rue de la Cavée, 92140 Clamart Cedex, France

[2]Department of Mathematics, University of British Columbia, 1984 Mathematics Road, Vancouver, BC, V6T 1Z2, Canada

[3]Department of Mechanical Engineering, University of British Columbia, 2324 Main Mall, Vancouver, BC, V6T 1Z4, Canada

[4]Dipartimento di Matematica, Universitá degli Studi, Viale Morgagni 67a, I-50134 Firenze, Italy

(Received 6 August 1999 and in revised form 4 February 2000)

In a plane-channel displacement flow of two visco-plastic fluids, it is possible for there to be a static residual layer of the displaced fluid left stuck to the walls of the channel. This phenomenon provides an idealized model for the formation of a *wet micro-annulus*, due to poor mud removal, during the primary cementing of an oil well. Using a lubrication approximation, it is shown that sufficient conditions for the non-existence of a static wall layer can be computed simply in terms of two dimensionless parameters: the Bingham number for the displacing fluid ($B_1$) and the ratio of the yield stresses of the two fluids ($\varphi_Y$). When these conditions are not met, it is possible to compute the maximum possible static wall layer thickness $h_{max}$, which depends on $B_1$, $\varphi_Y$ and on a third dimensionless parameter $\varphi_B$, a buoyancy to yield stress ratio.

On computing displacements using the lubrication approximation, the interface is observed to asymptotically approach the maximum static layer thickness as $t \to \infty$. Results from fully two-dimensional displacement computations are also presented. These indicate that the displacement front propagates at a steady speed along the channel, leaving behind a static layer which is significantly thinner than $h_{max}$. Surprisingly, the computed static layer thickness is observed to decrease with a parametric increase in the dimensionless yield stress of the displaced fluid. To explain these results we analyse the streamline configuration close to a steadily advancing displacement front. We demonstrate heuristically that the local visco-plastic dissipation functional will be approximately minimized by a critical layer thickness at which the displaced fluid begins to recirculate ahead of the displacement front. Comparison of the critical recirculation limit with the static layer thickness computed from the fully transient model gives a very close agreement, suggesting that a form of energy minimization is responsible in this case for selecting the static layer thickness.

## 1. Introduction

When a visco-plastic fluid flowing in a plane channel is displaced by a second visco-plastic fluid it is possible for there to be a static residual layer of the displaced

† Author to whom correspondence should be addressed.

fluid left stuck to the walls of the channel. This can occur only when the yield stress of the displaced fluid is larger than that of the displacing fluid. This is an essentially mechanical effect, which results when the yield stress of the displaced fluid is not exceeded at the wall of the channel. The study of this phenomenon is the focus of this paper. The principal question is: when can a static layer exist and what is its thickness? The practical importance of static residual layers in visco-plastic displacements stems from the process of mud removal during primary cementing of an oil well (as explained in § 1.2).

For simplicity, the two visco-plastic fluids are modelled as Bingham fluids. The fluids and displacement rates are assumed to be such that, although miscible, the fluids do not mix significantly on the timescale of the displacement. We also consider only flows for which the displacement front is symmetric with respect to the channel centreline. As such, the problem is one of the class of *finger width selection* problems typified by the well known Saffman–Taylor problem, (see for example Saffman & Taylor 1958; Saffman 1986; or the recently studied miscible version, Mineev-Weinstein 1998). There have been a number of recent studies of miscible displacements with Newtonian fluids in long ducts, without necessarily assuming a Hele-Shaw displacement. Those that focus on the high Péclet number limit of *low miscibility* are closest to our work (see for example Chen & Meiburg 1996; Lajeunesse *et al.* 1997, 1999; Lajeunesse 1999; Petitjeans & Maxworthy 1996; Yang & Yortsos 1997). Our approach is also partly motivated by the wish to avoid the complexities of modelling the physical properties of fluid mixtures when significant diffusion takes place (see for example Rogerson & Meiburg 1993*a*, *b*; Yortsos & Zeybek 1988; Zimmerman & Homsy 1991). Finally, in adopting a *classical* incompressible concentration-diffusion approach, we also ignore possible effects of Korteweg stresses and the effects of assuming a divergence-free velocity close to the displacement front. These effects are discussed by Joseph & Renardy (1993) and are hard to evaluate precisely.

Our intention is not to generalize the above Newtonian fluid studies (which are already complex) to the case of two passively advected Bingham fluids. Important phenomenological differences from the Newtonian fluid–fluid displacements exist. First, in a visco-plastic fluid–fluid displacement the residual wall layers are completely static. Second, the fully two-dimensional displacement allows properly steady finger propagation, i.e. of uniform width. Finally, the displacements considered are not Hele-Shaw displacements.

All Bingham fluid flow problems contain free surfaces, i.e. yield surfaces, and in this sense there is a weak analogy between the flow of a single Bingham fluid and any other free boundary problem. However, for simple transient Bingham flows the direct analogy is with a particular variant of the Stefan problem (see for example Comparini 1992; Frigaard, Howison & Sobey 1994). In geometries of large aspect ratio, as here, one is tempted to use lubrication-like approximations. Although such approximations do generally lead to valid approximations of the velocity field, the yield surfaces are often not well predicted. The underlying problem arises because the scaling arguments used to derive the leading-order momentum equations are not valid for velocity gradient terms in the unyielded flow regions. Two methodologies appear to correctly determine yield (and pseudo-yield) surface positions: that of Wilson and co-workers (Wilson 1993*a*, *b*; Wilson & Taylor 1996), and that used by Walton & Bittleston (1991).

Bingham fluid flows in which a second free surface or interface is involved have also been studied, and give rise to interesting physical phenomena. For example, free-surface flow of a Bingham fluid down a slope is studied in Liu & Mei (1989,

1994), wherein it is shown that, due to the plastic behaviour, a travelling localized pressure pulse can leave behind a permanent *footprint*. Footprinting of the static wall layers studied in this paper is also possible. The Saffman–Taylor fingering problem for a Bingham fluid has been considered by Alexandrou & Entov (1997) (see also the brief discussion in Wilson 1990), and shows that the fluid not displaced in a Hele-Shaw cell is properly static, i.e. between the propagating fingers. Although here we do not adopt the simplifications of the Hele-Shaw approach, the phenomenon of a static residual layer is quite analogous. In porous media or Hele-Shaw cells, visco-plastic displacements form one of a class of non-Darcy flows. Pascal has considered the displacement of oil in a reservoir by a visco-plastic fluid, see Pascal (1984*a*, *b*, 1986). Relevant non-Darcy flows are also described in Barenblatt, Entov & Ryzhik (1990). Flows of multiple Bingham fluids are not well understood and do not appear commonly in the open literature. A systematic study of flows that are associated with mechanical stability of a buoyancy-driven flow of two Bingham fluids is undertaken in Frigaard (1998), Frigaard & Scherzer (1998), Frigaard & Crawshaw (1999), Fenie & Frigaard (1999) and Frigaard & Scherzer (2000). However, these flows differ from those considered here in being axial flows in bounded domains satisfying a zero net flow rate constraint. The problems considered are mostly related to prescribing sufficient yield stresses in the two fluids in order to stop the flow.

### 1.1. *Outline*

The displacement flows we describe are extremely complex to study in generality. Thus, in this paper we focus exclusively on those displacements that leave behind a static residual wall layer of the displaced fluid. We apply a number of different analyses, all with the single aim of understanding for which dimensionless parameter values a static wall layer can exist and to try to predict its thickness. These questions have a practical industrial motivation, described in § 1.2, following.

Section 2 introduces the general displacement model that we wish to understand. The first analysis that yields relevant information is to consider an axial two-layer flow; see § 3. This simplified model helps to clarify exactly what is meant by a static residual wall layer and how this phenomenon arises naturally in a displacement. In parts of the displacement flow where the streamlines are *near-axial*, the axial two-layer model also provides the basis for a lubrication model of interface motion. It is shown that interface motion governed by the lubrication model will asymptotically approach the maximum possible static wall layer thickness; see § 3.3. We explore the parametric variation of the maximum static layer.

In § 4 we test the hypothesis that the maximum static layer thickness gives a good prediction of the actual static layer thickness, as computed from a fully two-dimensional transient model. A comparison is made over a wide range of dimensionless parameters, showing a large discrepancy between these two models.

A simple explanation for the difference is that the two-dimensional displacement flows generate larger shear stresses close to the displacement front than do the lubrication displacement flows. Since the maximal static layer represents the situation where the yield stress of the displaced fluid is attained exactly at the wall of the channel, any larger stresses generated must result in a thinner layer.

Although correct, this explanation does not lead to a simple prediction of static layer thickness for fully two-dimensional displacements. To this end, in § 5 we analyse a model for a steadily propagating two-dimensional displacement, leaving behind a uniform static layer. For this model, we show that the displaced fluid will recirculate

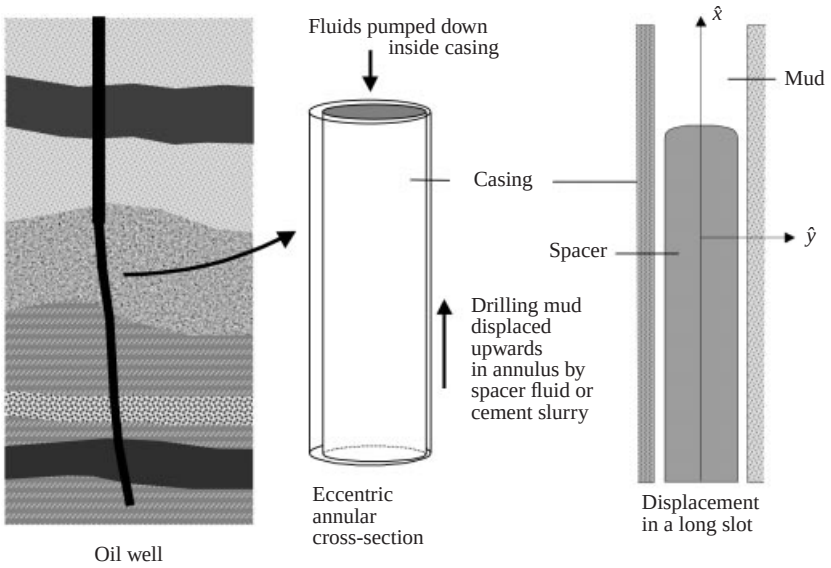


FIGURE 1. Primary cementing of an oil well. Fluid–fluid displacement in a narrow eccentric annulus. An azimuthal section of the annulus modelled simplistically as a long slot.

ahead of the displacement front for a sufficiently thin static layer. We argue heuristically that the visco-plastic dissipation rate, in the two-dimensional region local to the advancing displacement front, will be minimized by a static layer thickness that is just above the maximal layer for which recirculation occurs. This *recirculation* limiting layer thickness is found to give a very good quantitative prediction of computed static layer thickness over a range of dimensionless parameters; see § 5.2. The paper ends with a brief summary and discussion in § 6.

### 1.2. *Primary cementing of an oil well*

The potential for there to exist static residual layers of displaced visco-plastic fluid is of enormous practical significance in the primary cementing of an oil well. In this process a sequence of fluids are pumped through a narrow eccentric annulus in an effort to displace the drilling mud (for process details see Guillot *et al.* 1990; Smith 1987). The displacing fluid is typically either a *spacer* fluid or the leading cement slurry. The annular gap is formed by the outside wall of the steel casing, which is to be cemented in place, and the inside wall of the drilled rock formation, see figure 1. The practical problem with leaving a mud layer on the walls of the annulus occurs when the cement slurry sets. The layer of mud that is left stuck to the walls of the annulus can extend axially along the annulus, connecting different fluid-bearing regions of the rock formation: a so-called *wet micro-annulus*. This mud layer is typically much more permeable than the set cement, and particularly so in the case of a water-based drilling mud since the process of cement setting is strongly exothermic and also hydrophilic. Zonal isolation is destroyed by the micro-annular layer and the consequent pressure drop in the oil reservoir can severely damage the productivity of the well; see Economides (1990).

A number of workers have analysed the axial flow of visco-plastic fluids in an eccentric annulus (see for example Szabo & Hassager 1992; Walton & Bittleston 1991). However, these studies are confined to axial flows of a single fluid. For Newtonian

displacements, three-dimensional displacement simulations have also been carried out by Szabo & Hassager (1997). In cementing, typical ratios of mean annular gap to mean diameter are $< 0.1$ and the ratio of mean annular gap to an axial length scale (here taken as the length of a casing stand) is $\approx 0.002$. Thus, representing the narrow annulus as an azimuthal series of long plane channels (slot-approximation) is quite reasonable, and is a common practice in modelling cementing flows. Whilst this ignores azimuthal flows, it provides a key building block for understanding the annular displacement. Only laminar displacements are considered. Different pumping rates are employed in primary cementing, but often turbulent flow is not attainable. In an eccentric annulus the fluids move significantly slower on the narrow side of the annulus than on the wide side (even stopping). Poor mud removal is commonly associated with the narrow side of the annulus. Typical (narrow side) velocity scales $\hat{U}_0$ would be between 1 and 30 cm s$^{-1}$. The annular-gap length scale is $\hat{D} \sim 1$ cm.

The fluids involved can be modelled as visco-plastic generalized Newtonian fluids, (e.g. Bingham fluids, Herschel–Bulkley fluids, Casson fluids). Spacers do not always exhibit a yield stress, visco-elasticity can be important in different situations and, when static, a gel strength usually develops in the mud. These complications apart, visco-plasticity is a key feature of these fluids and is that feature believed to be most relevant to the phenomenon of static wall layers. The simplified characterization of these fluids by the Bingham fluid model is used regularly in the oil industry. Validity of the assumption of miscibility depends on whether the two fluids are water-based or oil-based, but is often the case. When miscible, the Péclet number is in the range $Pe > 10^6$. Densities of the fluids can range anywhere between 1000 and 2000 kg m$^{-3}$, with typical density differences between displacing and displaced fluids in the range 50–300 kg m$^{-3}$. Characteristic yield stresses are of the order of 1 to 20 Pa and plastic viscosities commonly in the range 5 to 100 cP. Extreme rheological parameters can also occur and an underlying reason for studying this phenomenon is to assess in which ways *badly conditioned* fluids can affect the mud removal process.

## 2. Laminar two-dimensional miscible displacements

We consider a two-dimensional geometry between two parallel plates, separated by a distance $2\hat{D}$, i.e. a slot. The slot is initially filled with fluid 2, which is displaced by fluid 1, injected at $\hat{x} = 0$ with a mean velocity $\hat{\boldsymbol{u}}(0, \hat{t}) = (\hat{U}_0, 0)$. Cartesian coordinates $(\hat{x}, \hat{y})$ are as shown in figure 1. The scale of the slot in the $\hat{x}$-direction is assumed to be such that $\hat{x} \sim \hat{L}$, where $\hat{D} \ll \hat{L}$.

The densities of the fluids are denoted $\hat{\rho}_k : k = 1, 2$. Iso-density ($\hat{\rho}_1 = \hat{\rho}_2$) or buoyant displacements ($\hat{\rho}_1 > \hat{\rho}_2$) will be considered. We restrict attention to situations where the displacement flow is symmetric about the slot centreline $\hat{y} = 0$. Physically, this assumption corresponds to a buoyant upward displacement in a vertical slot, or to an iso-density displacement in a slot of any orientation. The displacement flows are always assumed laminar and the symmetry assumption implies that inertial effects are not dominant, (i.e. in the sense that we are assuming no symmetry-breaking of the basic flow), but not necessarily negligible either. Although miscible, the case of zero diffusion is considered, which is formally equivalent to an immiscible displacement with no surface tension. In this case, the two fluids are delineated by a sharp interface, which can be modelled straightforwardly with either a kinematic equation or by a passive scalar (concentration) that is advected with the fluid (no diffusion).

The velocity, pressure and deviatoric stress are denoted $\hat{\boldsymbol{u}}(\hat{\boldsymbol{x}},\hat{t}) \equiv (\hat{u},\hat{v}) \equiv (\hat{u}_1,\hat{u}_2)$, $\hat{p}_k(\hat{\boldsymbol{x}},\hat{t})$ and $\hat{\tau}_{k,ij}$, respectively. The equations of motion, valid within each fluid region $V_k, k = 1,2$, are

$$\hat{\rho}_k\left[\frac{\partial\hat{u}}{\partial\hat{t}} + \hat{u}\frac{\partial\hat{u}}{\partial\hat{x}} + \hat{v}\frac{\partial\hat{u}}{\partial\hat{y}}\right] = -\frac{\partial\hat{p}_k}{\partial\hat{x}} + \frac{\partial}{\partial\hat{x}}\hat{\tau}_{k,xx} + \frac{\partial}{\partial\hat{y}}\hat{\tau}_{k,xy} - \hat{\rho}_k\hat{g}, \tag{2.1}$$

$$\hat{\rho}_k\left[\frac{\partial\hat{v}}{\partial\hat{t}} + \hat{u}\frac{\partial\hat{v}}{\partial\hat{x}} + \hat{v}\frac{\partial\hat{v}}{\partial\hat{y}}\right] = -\frac{\partial\hat{p}_k}{\partial\hat{y}} + \frac{\partial}{\partial\hat{x}}\hat{\tau}_{k,yx} + \frac{\partial}{\partial\hat{y}}\hat{\tau}_{k,yy}, \tag{2.2}$$

$$\frac{\partial\hat{u}}{\partial\hat{x}} + \frac{\partial\hat{v}}{\partial\hat{y}} = 0. \tag{2.3}$$

On the wall of the slot the no-slip condition is satisfied:

$$\hat{\boldsymbol{u}}(\hat{x},\hat{D}) = 0, \tag{2.4}$$

and on the centreline, from the assumption of symmetry:

$$\frac{\partial\hat{u}}{\partial\hat{y}}(\hat{x},0) = \hat{v}(\hat{x},0) = 0. \tag{2.5}$$

The interface is denoted $\hat{y} = \hat{Y}_i(\hat{x},\hat{t})$, and is simply advected with the flow:

$$\frac{\partial\hat{Y}_i}{\partial\hat{t}} + \hat{u}\frac{\partial\hat{Y}_i}{\partial\hat{x}} = \hat{v}. \tag{2.6}$$

Across the interface, velocity and stress are continuous.

The rheologies assumed are those of Bingham fluids. Rate of strain and deviatoric stress second invariants, $\hat{\dot{\gamma}}(\hat{\boldsymbol{u}})$ and $\hat{\tau}_k(\hat{\boldsymbol{u}})$ respectively, are defined by

$$\hat{\dot{\gamma}}(\hat{\boldsymbol{u}}) = \left[\frac{1}{2}\sum_{i,j=1}^{2}[\hat{\dot{\gamma}}_{ij}(\hat{\boldsymbol{u}})]^2\right]^{1/2}, \tag{2.7}$$

$$\hat{\tau}_k(\hat{\boldsymbol{u}}) = \left[\frac{1}{2}\sum_{i,j=1}^{2}[\hat{\tau}_{k,ij}(\hat{\boldsymbol{u}})]^2\right]^{1/2}, \tag{2.8}$$

where

$$\hat{\dot{\gamma}}_{ij}(\hat{\boldsymbol{u}}) = \frac{\partial\hat{u}_i}{\partial\hat{x}_j} + \frac{\partial\hat{u}_j}{\partial\hat{x}_i}. \tag{2.9}$$

Constitutive laws for the Bingham fluids are

$$\hat{\dot{\gamma}}(\hat{\boldsymbol{u}}) = 0 \Longleftrightarrow \hat{\tau}_k(\hat{\boldsymbol{u}}) \leqslant \hat{\tau}_{k,Y}, \quad \hat{\boldsymbol{x}} \in V_k, \tag{2.10}$$

$$\hat{\tau}_{k,ij}(\hat{\boldsymbol{u}}) = \left[\hat{\mu}_k + \frac{\hat{\tau}_{k,Y}}{\hat{\dot{\gamma}}(\hat{\boldsymbol{u}})}\right]\hat{\dot{\gamma}}_{ij}(\hat{\boldsymbol{u}}) \Longleftrightarrow \hat{\tau}_k(\hat{\boldsymbol{u}}) > \hat{\tau}_{k,Y}, \quad \hat{\boldsymbol{x}} \in V_k. \tag{2.11}$$

The constants $\hat{\mu}_k$ and $\hat{\tau}_{k,Y}$ are the plastic viscosity and yield stress, respectively, for each fluid; $k = 1,2$. These parameters are assumed to be strictly positive.

### 2.1. *Scaled equations*

Dimensionless equations are defined via the following scaling:

$$\left.\begin{aligned} \hat{\boldsymbol{x}} &= \hat{D}\boldsymbol{x}, & \hat{\boldsymbol{u}} &= \hat{U}_0\boldsymbol{x}, \\ \hat{t} &= \frac{\hat{D}}{\hat{U}_0}t, & \hat{\dot{\gamma}}_{ij} &= \frac{\hat{U}_0}{\hat{D}}\dot{\gamma}_{ij}, \\ \hat{p}_k &= \hat{\rho}_2\hat{U}_0^2 p_k, & \hat{\tau}_{k,ij} &= \hat{\rho}_2\hat{U}_0^2\tau_{k,ij}, \\ \hat{Y}_i &= \hat{D}Y_i. \end{aligned}\right\} \tag{2.12}$$

The equations of motion are

$$r_k\left[\frac{\partial u}{\partial t}+u\frac{\partial u}{\partial x}+v\frac{\partial u}{\partial y}\right]=-\frac{\partial p_k}{\partial x}+\frac{\partial}{\partial x}\tau_{k,xx}+\frac{\partial}{\partial y}\tau_{k,xy}-\frac{r_k}{F}, \tag{2.13}$$

$$r_k\left[\frac{\partial v}{\partial t}+u\frac{\partial v}{\partial x}+v\frac{\partial v}{\partial y}\right]=-\frac{\partial p_k}{\partial y}+\frac{\partial}{\partial x}\tau_{k,yx}+\frac{\partial}{\partial y}\tau_{k,yy}, \tag{2.14}$$

$$\frac{\partial u}{\partial x}+\frac{\partial v}{\partial y}=0. \tag{2.15}$$

The kinematic equation for the interface is:

$$\frac{\partial Y_i}{\partial t}+u\frac{\partial Y_i}{\partial x}=v, \tag{2.16}$$

and scaled constitutive laws are now

$$\dot{\gamma}(\boldsymbol{u})=0 \Longleftrightarrow \tau_k(\boldsymbol{u})\leqslant\tau_{k,Y}, \quad \boldsymbol{x}\in V_k, \tag{2.17}$$

$$\tau_{k,ij}(\boldsymbol{u})=\left[\mu_k+\frac{\tau_{k,Y}}{\dot{\gamma}(\boldsymbol{u})}\right]\dot{\gamma}_{ij}(\boldsymbol{u}) \Longleftrightarrow \tau_k(\boldsymbol{u})>\tau_{k,Y}, \quad \boldsymbol{x}\in V_k. \tag{2.18}$$

Noting that $r_2\equiv 1$, there are six dimensionless parameters in (2.13)–(2.18): the density ratio $r$

$$r\equiv\frac{\hat{\rho}_1}{\hat{\rho}_2}=r_1, \tag{2.19}$$

the Froude number

$$F\equiv\frac{\hat{U}_0^2}{\hat{g}\hat{D}}, \tag{2.20}$$

and the dimensionless yield stresses and plastic viscosities

$$\tau_{k,Y}\equiv\frac{\hat{\tau}_{k,Y}}{\hat{\rho}_2\hat{U}_0^2}, \quad \mu_k\equiv\frac{\hat{\mu}_k}{\hat{\rho}_2\hat{U}_0\hat{D}}. \tag{2.21}$$

The boundary and interface conditions are unchanged, but note that the choice of velocity scale implies that $u$ has unit mean value. Values of the six dimensionless parameters $r$, $F$, $\tau_{k,Y}$, $\mu_k$, $k=1,2$, that might be found in a typical cementing process are hard to define precisely, due to the wide range of fluid properties and variations in $\hat{D}$ and $\hat{U}_0$ at different azimuthal positions in an eccentric annulus. However, we only seek to study the phenomenon of a static wall layer. For our computations we have implicitly assumed $r\geqslant 1$, $F\sim 10^{-3}$–$10^{-1}$, $\tau_{k,Y}\in[0.05,5]$, $\mu_k\in[0.0005,0.1]$, for both $k=1$ and 2; moreover, $\tau_{2,Y}>\tau_{1,Y}$ and $\mu_2>\mu_1$ is common for static wall layers.

## 3. Axial displacement flows

The principal aim of the paper is to understand the phenomenon of a static residual wall layer left behind after an incomplete displacement. The first useful analysis comes from considering axial two-layer flows. For flows in long ducts, it is quite natural to consider situations when the streamlines and interface align approximately with the duct walls. Even in two-dimensional displacement flows there are likely to be parts of the flow which are near-axial, e.g. when the displacement front has passed a given point and the interface elongates behind the front. Thus, axial two-layer flows represent a good starting point at which to develop our understanding of static wall layer solutions to equations (2.13)–(2.18).

We first examine the range of possible velocity profiles for a two-layer flow. This leads naturally to the definition of a maximal static residual wall layer in § 3.2. In § 3.3, we consider an axial displacement model that is based on the two-layer flow and show that, for dimensionless parameter values that allow static wall layers, the interface approaches the maximal static layer thickness asymptotically. Thus, for such a model of the displacement process, the maximal layer is an excellent prediction of the *actual* layer thickness observed in a transient displacement. More realistic displacement models are treated in § 4 and following.

### 3.1. *Two-layer flows*

It is straightforward to derive an axial two-layer model from (2.13)–(2.18). At leading order there is no pressure gradient across the slot and the $x$-momentum equations describe an axial two-fluid shear flow:

$$\frac{\mathrm{d}}{\mathrm{d}y}\tau_{1,xy} = b - f, \quad y \in [0, Y_i), \tag{3.1}$$

$$\frac{\mathrm{d}}{\mathrm{d}y}\tau_{2,xy} = -f, \quad y \in (Y_i, 1]. \tag{3.2}$$

Here the interface position is denoted simply by $y = Y_i$. The two new parameters are $b$, the buoyancy number, and $f$ the modified pressure gradient:

$$b \equiv \frac{r-1}{F}, \quad f \equiv -\frac{\mathrm{d}p}{\mathrm{d}x} - \frac{1}{F}. \tag{3.3}$$

Equations (3.1) and (3.2) are solved to give the leading-order axial velocity, $(u, v) \sim (U(y), 0)$, using the following boundary and interface conditions:

$$\tau_{1,xy}(0) = 0, \tag{3.4}$$

$$\tau_{1,xy}(Y_i) = \tau_{2,xy}(Y_i), \tag{3.5}$$

$$U(Y_i^+) = U(Y_i^-), \tag{3.6}$$

$$U(1) = 0. \tag{3.7}$$

Simplified constitutive equations are

$$|U_y| = 0 \Longleftrightarrow |\tau_{k,xy}| \leqslant \tau_{k,Y}, \tag{3.8}$$

$$\tau_{k,xy} = \left[\mu_k + \frac{\tau_{k,Y}}{|U_y|}\right] U_y \Longleftrightarrow |\tau_{k,xy}| > \tau_{k,Y}. \tag{3.9}$$

Because the velocity scaling has been chosen as the mean displacement velocity, the following condition must also be satisfied:

$$\int_0^1 U(y)\mathrm{d}y = 1. \tag{3.10}$$

Constraint (3.10) is used to define $f$ and the solution to (3.1)–(3.10) is consequently the pair $(U, f)$. The results in Frigaard & Scherzer (1998) can be applied to show that there exists a unique solution $(U, f)$ to this system for each value of $Y_i \in [0, 1]$. Integrating (3.1) and (3.2) gives

$$\tau_{1,xy} = (b - f)y, \quad y \in [0, Y_i], \tag{3.11}$$

$$\tau_{2,xy} = bY_i - fy, \quad y \in (Y_i, 1]. \tag{3.12}$$

The velocity profiles that result from these stress distributions depend entirely on the intercept of the linear stress functions with the two yield stress values, i.e. where $\tau_{k,xy} = \pm\tau_{k,Y}$. There is clearly a limited number of configurations that give rise to qualitatively different velocity profiles. For completely arbitrary values of $f$ and $b$, without the constraint (3.10), there are in fact 21 qualitatively different velocity profiles possible (excluding marginal cases where either $f = 0$ or $f = b$).

Here we are interested primarily in flows for which a flow rate is imposed, see (3.10), for which the displacing fluid is heavier than the displaced fluid ($b \geqslant 0$), and for which both fluids are being *pushed* in the positive direction ($f > b$). Under such conditions, only four qualitatively different velocity profiles remain feasible. These are shown schematically in figure 2.

The velocity profile shown in figure 2($a$) is unique amongst those in figure 2, in that fluid 2, adjacent to the wall at $y = 1$, does not move. The yield stress of fluid 2 is not exceeded at the wall, or anywhere within the fluid-2 layer, and the condition of no-slip accomplishes the rest. This velocity profile is the archetypal static-wall-layer velocity profile that we study throughout this paper.

Static layers in a two-layer flow are relatively easy to find in the parameter space $(b, \tau_{k,Y}, \mu_k)$: $k = 1, 2$. In essence they occur if the yield stress of fluid 2 is significantly larger than that of fluid 1. However, for given rheological parameters not every interface position can give a static wall layer. Suppose that (3.10) is satisfied and the set of rheological parameters $(b, \tau_{k,Y}, \mu_k)$: $k = 1, 2$, are fixed. Typically, the velocity profiles close to $Y_i = 0$ resemble those in figure 2($c$). For intermediate values of $Y_i$ the *double Bingham–Poiseuille* profile of figure 2($b$) is commonly found and close to the wall figure 2($a$) is found. The profile in figure 2($d$) is a variant of figure 2($b$), observed if $\tau_{2,Y}$ is relatively weak.

### 3.2. *Maximum static wall layer thickness*

Suppose that we have fixed dimensionless parameters $(b, \tau_{k,Y}, \mu_k)$: $k = 1, 2$, for which a velocity profile such as that in figure 2($a$) exists if $Y_i \sim 1$. Now consider the variation in this velocity profile as $Y_i$ decreases. Imposing the constraint (3.10) means that the same flow rate of fluid 1 is forced through a progressively narrower gap. As the gap narrows, if fluid 2 remains static, the modified pressure gradient $f$ increases (for a Newtonian fluid: $f \sim Y_i^{-1}$, and $f \to \infty$ faster for a Bingham fluid). For each $Y_i$, the wall shear stress $\tau_w \equiv \tau_{2,xy}(1)$ is given by

$$\tau_w = -f + bY_i, \tag{3.13}$$

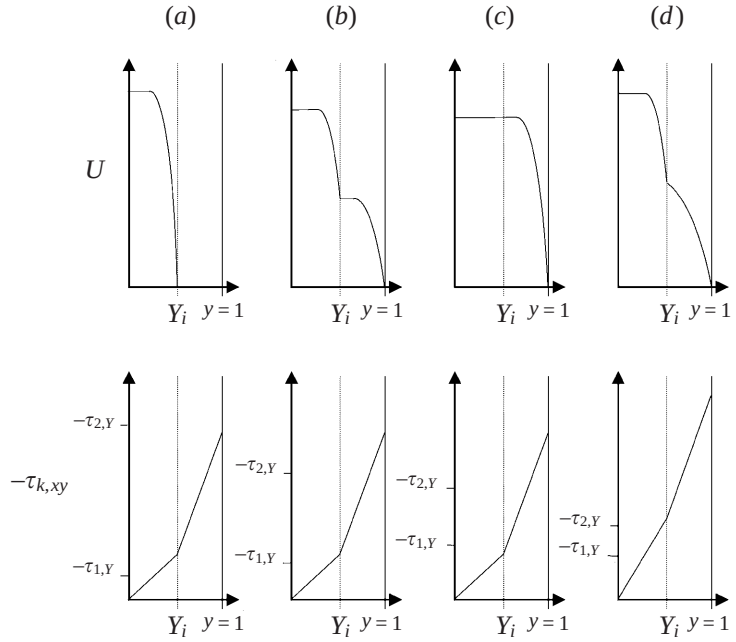


FIGURE 2. Schematic of the different possible characteristic axial velocity profiles for positive buoyant displacements ($f > b \geqslant 0$).

and thus $\tau_w \sim -f \to -\infty$ as $Y_i \to 0$. For small enough $Y_i$ any finite $\tau_{2,Y}$ will be exceeded by the wall shear stress. In other words, there will be a minimal interface position $Y_{i,min}$ for which the fluid-2 layer is able to remain static. The thickness of the maximum possible static wall layer, $h_{max}$, is formally defined by

$$h_{max} \equiv 1 - Y_{i,min}. \tag{3.14}$$

It is easy to determine the value of $Y_{i,min}$ (i.e. $h_{max}$) for any set of parameters.

With reference to figure 2(*a*), it can be seen that when a static layer exists, the velocity profile is equivalent to that of a single Bingham fluid flowing through a slot of half-width $Y_i$. Denote by $f_0(Y_i)$ the value of the modified pressure gradient necessary to force a unit flow rate of fluid 1 through a slot of half-width $Y_i$. Thus, $(U, f_0)$ satisfies

$$\frac{\mathrm{d}}{\mathrm{d}y}\tau_{1,xy} = b - f_0, \quad y \in [0, Y_i], \tag{3.15}$$

$$\tau_{1,xy}(0) = 0, \tag{3.16}$$

$$U(Y_i) = 0, \tag{3.17}$$

$$\int_0^{Y_i} U(y)\mathrm{d}y = 1. \tag{3.18}$$

The solution $(U, f_0)$ of (3.15)–(3.18) is identical to the restriction to $y \in [0, Y_i]$ of the solution $(U, f)$ of the full problem (3.1)–(3.10), provided that there exists a static wall layer in fluid 2.

The absolute value of the shear stress increases throughout the fluid-2 layer, so that the yield stress in fluid 2 will be first exceeded at the wall. It follows that a necessary

and sufficient condition for there to be static wall layer solutions is that

$$f_0(1) - b < \tau_{2,Y}, \tag{3.19}$$

and that $Y_{i,min}$ will be defined by

$$f_0(Y_{i,min}) - Y_{i,min} b = \tau_{2,Y}. \tag{3.20}$$

The solution to (3.15)–(3.17) is well known. For $Y_i(f_0 - b) > \tau_{1,Y}$, the positive (areal) flow rate, $q_{1,single}$, is given by

$$q_{1,single}(Y_i, f_0) = \frac{[2Y_i(f_0 - b) + \tau_{1,Y}][Y_i(f_0 - b) - \tau_{1,Y}]^2}{6\mu_1(f_0 - b)^2}. \tag{3.21}$$

In order that (3.18) be satisfied, $q_{1,single}(Y_i, f_0) = 1$, for any $Y_i \geqslant Y_{i,min}$. After a little algebra, $f_0(Y_i)$ is found from

$$\frac{(f_0 - b)Y_i}{\tau_{1,Y}} = \xi(\tilde{B}_1), \tag{3.22}$$

where $\tilde{B}_1$ is a modified fluid-1 Bingham number, defined by

$$\tilde{B}_1 = {Y_i}^2 \frac{\tau_{1,Y}}{\mu_1}, \tag{3.23}$$

and $\xi(B)$ is the only root of

$$2\xi^3 - (3 + 6/B)\xi^2 + 1 = 0, \tag{3.24}$$

lying in $\xi(B) > 1$ for $B > 0$. It is straightforward to see that

$$(1 + 2/B) < \xi(B) < \tfrac{3}{2}(1 + 2/B), \tag{3.25}$$

and hence $\xi(B)$ is easily computed, see figure 3. Differentiating (3.24) gives

$$\frac{\mathrm{d}\xi(B)}{\mathrm{d}B} = \frac{\xi(B)}{B^2[(1 + 2/B) - \xi(B)]} < 0. \tag{3.26}$$

Thus, $f_0 - b$ is seen to depend on three parameters: the interface position $Y_i$, the fluid-1 yield stress and the fluid-1 Bingham number $B_1$:

$$B_1 = \frac{\tau_{1,Y}}{\mu_1}. \tag{3.27}$$

Note that $(f_0 - b)/\tau_{1,Y}$ decreases monotonically as a function of each of $(Y_i, B_1)$.

We can rewrite $\xi(\tilde{B}_1) \equiv \xi(B_1, Y_i)$, using (3.23) and (3.27). Returning to (3.20), we divide through by $\tau_{2,Y}$ to finally give

$$\frac{\tau_{1,Y}}{\tau_{2,Y}} \frac{\xi(B_1, Y_{i,min})}{Y_{i,min}} + (1 - Y_{i,min}) \frac{b}{\tau_{2,Y}} = 1. \tag{3.28}$$

From (3.28) it follows that the maximum layer thickness is governed only by three dimensionless parameters:

$$\varphi_Y = \frac{\tau_{1,Y}}{\tau_{2,Y}} \equiv \frac{\hat{\tau}_{1,Y}}{\hat{\tau}_{2,Y}}, \tag{3.29}$$

$$B_1 = \frac{\tau_{1,Y}}{\mu_1} \equiv \frac{\hat{\tau}_{1,Y}\hat{D}}{\hat{\mu}_1 \hat{U}_0}, \tag{3.30}$$

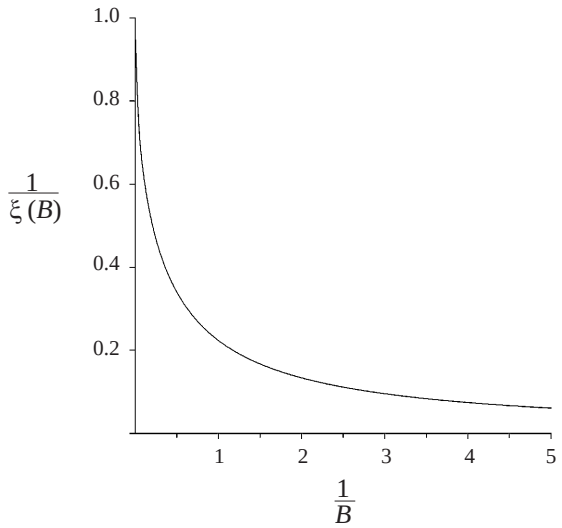


FIGURE 3. The function $1/\xi(B)$ plotted against $1/B$.

$$\varphi_B = \frac{b}{\tau_{2,Y}} \equiv \frac{(\hat{\rho}_1 - \hat{\rho}_2)\hat{g}\hat{D}}{\hat{\tau}_{2,Y}}. \tag{3.31}$$

Note that since fluid 1 must yield in the case of a static wall layer, $\varphi_Y < 1$. The Bingham number $B_1$ compares plastic and viscous stresses in fluid 1. The ratio $\varphi_B$ measures the buoyancy force (stress) against the ability of the fluid-2 layer to resist motion. Figure 4 shows the variation in $h_{max}$ with the parameters $\varphi_Y$ and $1/B_1$ for four fixed values of the ratio $\varphi_B$. The shaded area marks the limit where no static wall layers are possible. Increasing either $\varphi_Y$ or $\varphi_B$ decreases the maximum static wall layer, whilst increasing $B_1$ has the effect of increasing $h_{max}$. Note that an increase in $B_1$, while leaving $\tau_{1,Y}$ fixed, necessitates a decrease in the plastic viscosity of fluid 1, decreasing the shear stress.

The critical condition (3.19), defining whether or not there can exist a static wall layer, is seen to be entirely independent of the buoyancy ratio $\varphi_B$, and is given very simply by

$$\varphi_Y = \frac{1}{\xi(B_1, 1)}, \tag{3.32}$$

i.e. for each fluid-1 Bingham number $B_1$ there is a critical yield stress ratio, above which no static wall layer can persist. Physically, the number $1/\xi(B_1, 1)$ will give the ratio of the fluid-1 yield surface thickness to the slot width, in a Bingham–Poiseuille flow of fluid 1 with mean velocity $\hat{U}_0$, that occupies the entire slot. The ratio $\varphi_Y$ must exceed this geometric ratio for there to be no static wall layer. Figure 5 plots the critical curve (3.32).

### 3.3. *Interface propagation for axial displacements*

Having defined $h_{max}$ via the two-layer model, the question arises as to whether or not $h_{max}$ provides an indication of the static layer thickness observed in any physically realistic displacement. In situations where the interface and streamlines are near-axial, a simple model for interface motion can be derived. The interface position is denoted $y = Y_i(x, t)$ and the interface is a material surface that moves according to

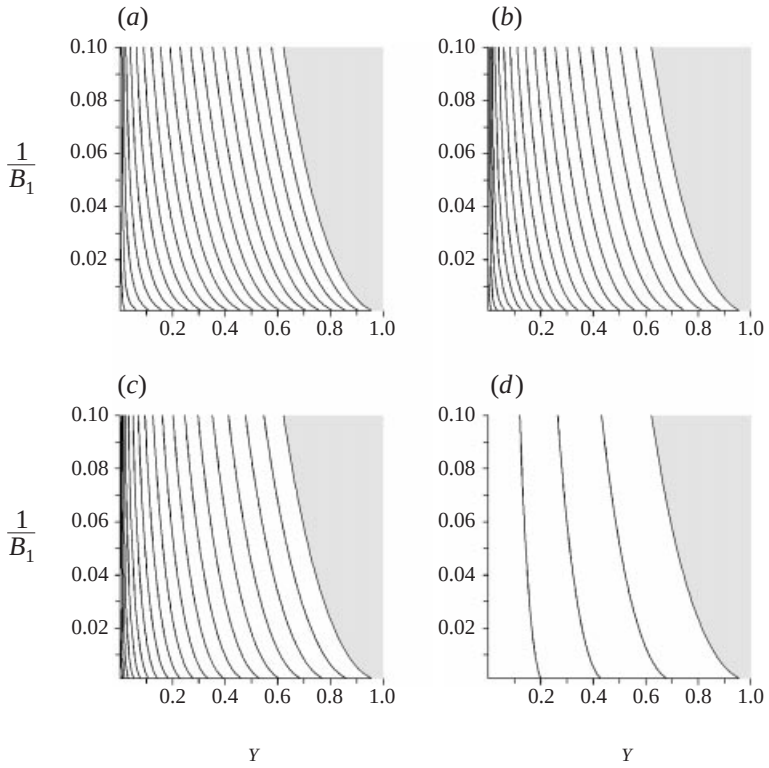


FIGURE 4. Maximal static wall layer $h_{max}$ for $\varphi_Y \in [0.001, 1]$, $1/B_1 \in [0.001, 0.1]$; contours spaced at intervals $\Delta h_{max} = 0.05$: (*a*) $\varphi_B = 0.0$; (*b*) $\varphi_B = 0.5$; (*c*) $\varphi_B = 1.0$; (*d*) $\varphi_B = 2.0$.

the kinematic equation:

$$\frac{\partial Y_i}{\partial t} + U\frac{\partial Y_i}{\partial x} = V. \tag{3.33}$$

Here the axial velocity $U$ comes from (3.1)–(3.10) and the cross-stream velocity component $V$ can then be reconstructed from

$$\frac{\partial V}{\partial y} = -\frac{\partial U}{\partial x}. \tag{3.34}$$

This approach is very classical: $(x, t)$-dependence enters into (3.1)–(3.10) only through the interface position, i.e. $U(x, y, t) \equiv U(Y_i(x, t), y)$. Combining (3.33) and (3.34) leads to the following first-order hyperbolic equation:

$$\frac{\partial Y_i}{\partial t} + \frac{\partial}{\partial x} q_1(Y_i) = 0, \tag{3.35}$$

where the flux function $q_1(Y_i)$ is defined by

$$q_1(Y_i) \equiv \int_0^{Y_i} U(x, y, t)\mathrm{d}y. \tag{3.36}$$

We now solve equation (3.35) for parameters $(b, \tau_{k,Y}, \mu_k)$: $k = 1, 2$, for which velocity profiles such as in figure 2(*a*) can result.

Numerically, we construct $q_1(Y_i)$ by solving the system (3.1)–(3.10) for $N_{Y_i} = 100$ evenly spaced values of $Y_i \in [0, 1]$ and then by using linear interpolation. Equation

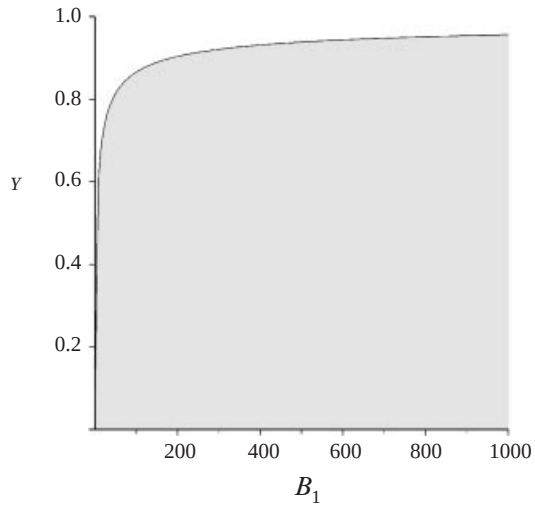


FIGURE 5. Critical yield stress ratio $\varphi_Y$ below which a static layer can exist, plotted against $B_1$; static layers exist in the shaded region.

(3.35) is integrated from given initial conditions. The method we use for (3.35) is due to Cockburn & Shu (1994) and is a compact differencing scheme that is nonlinearly stable and third order in both time and space. The solutions to (3.35) often become discontinuous in time (i.e. shocks form) and the method in Cockburn & Shu (1994) is designed to be *shock-capturing*. Apart from the test problems in Cockburn & Shu (1994), this method has been used previously in Fenie & Frigaard (1999) for a similar problem of interface propagation with shock discontinuities and was found to perform well.

Examples of iso-density displacements are shown in figures 6 and 7, for two different parameter sets:

$$(b, \tau_{1,Y}, \tau_{2,Y}, \mu_1, \mu_2) = (0, 0.2, 0.5, 0.01, 0.05),$$
$$(b, \tau_{1,Y}, \tau_{2,Y}, \mu_1, \mu_2) = (0, 0.2, 1.0, 0.005, 0.01).$$

We have used initial conditions:

$$Y_i(x,0) = \begin{cases} 1, & x < 1 \\ 2 - x, & x \in [1,2] \\ 0, & x > 2. \end{cases}$$

Figures 6 and 7 show the interface positions at successive time intervals, as indicated. The functions $q_1(Y_i)$, $f(Y_i)$ and $\tau_i(Y_i)$ are also shown, the latter denoting the interfacial shear stress.

As the interface propagates it clearly approaches a certain layer thickness (the approach is much slower in figure 6 than in figure 7). This interface position is that at which $q_1(Y_i) \to 1$. We recall that the solution $(U, f_0)$ of (3.15)–(3.18) is identical to the restriction to $y \in [0, Y_i]$ of the solution $(U, f)$ of (3.1)–(3.10), for exactly those interface positions that admit a static wall layer. By definition, $q_1(Y_i) = 1$ for these interface positions. We can therefore conclude that the limiting interface position is $Y_i = Y_{i,min}$, i.e. the maximum layer thickness is approached by the interface, as is confirmed numerically. Additionally, at the limiting layer thickness, $q_1'(Y_i) \to 0$, and therefore the approach of $Y_i \to Y_{i,min}$ is asymptotic as $t \to \infty$.

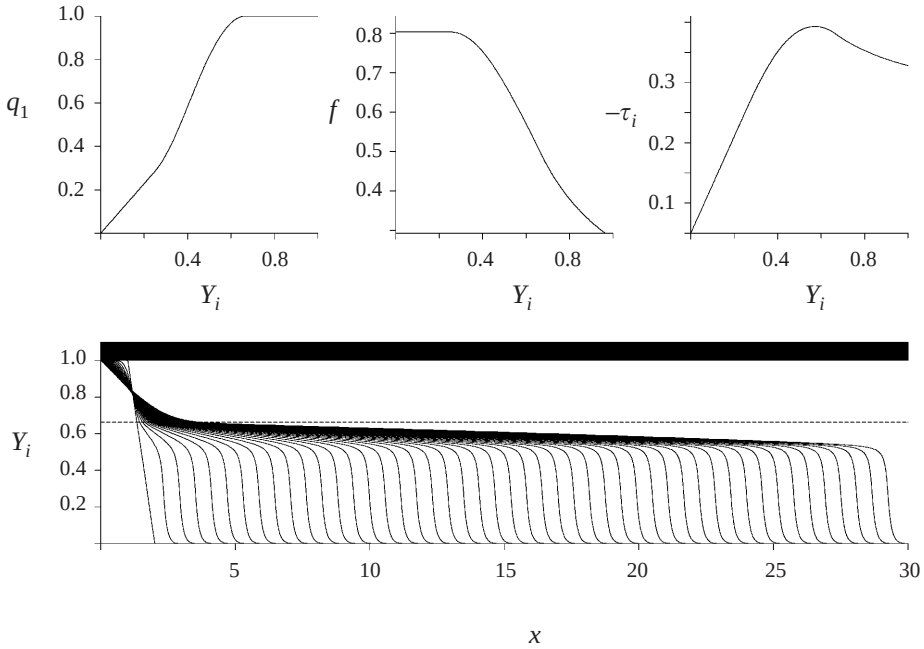


FIGURE 6. Axial displacement for $(b, \tau_{1,Y}, \tau_{2,Y}, \mu_1, \mu_2) = (0, 0.2, 0.5, 0.01, 0.05)$. The functions $q_1(Y_i)$, $f(Y_i)$ and $\tau_i(Y_i)$. Interface propagation plotted every 100 timesteps; computation on a mesh of size $\Delta z = 0.02$ with a timestep $\Delta t = 0.0035$.

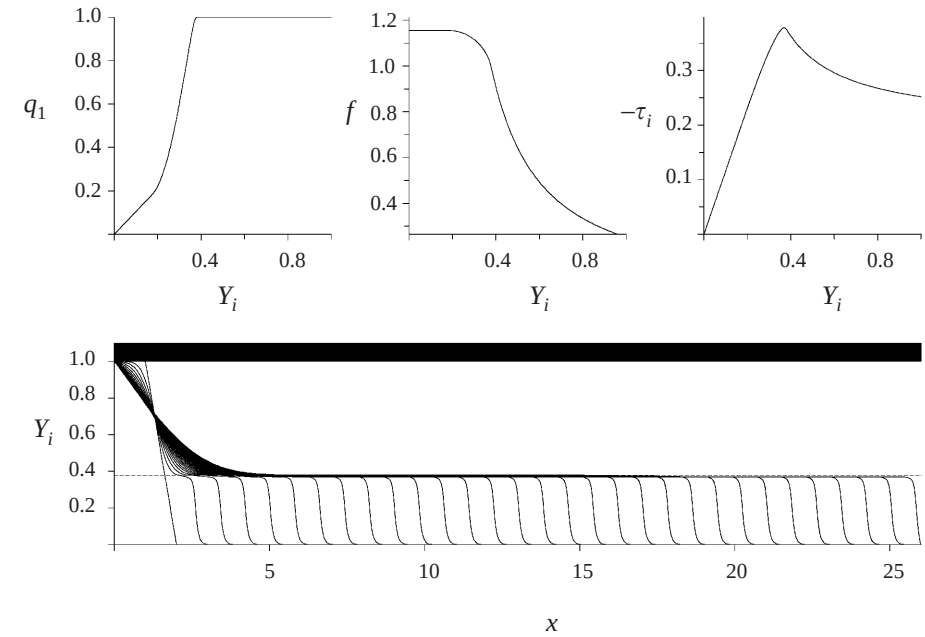


FIGURE 7. Axial displacement for $(b, \tau_{1,Y}, \tau_{2,Y}, \mu_1, \mu_2) = (0, 0.2, 1.0, 0.005, 0.01)$. The functions $q_1(Y_i)$, $f(Y_i)$ and $\tau_i(Y_i)$. Interface propagation plotted every 200 timesteps; computation on a mesh of size $\Delta z = 0.02$ with a timestep $\Delta t = 0.0015$.

In both figures 6 and 7 the central part of the displacement front (small $Y_i$) is propagating as a shock discontinuity. Smoothing effects observed in figures 6 and 7, both close to the shock and close to the inflow, are a numerical effect characteristic of the scheme in Cockburn & Shu (1994) (and many other shock-capturing methods). Note that for small $Y_i$ the solution $f(Y_i)$ is constant. For these interface values the axial velocity profile is schematically as in figure 2($c$); fluid 1 is entirely unyielded, as is fluid 2 at the interface, and it is irrelevant which fluid occupies the central part of the channel. The decline in $f(Y_i)$ marks the transition from axial solutions as shown in figure 2($c$) to those shown in figure 2($b$). The transition to static layer solutions (figure 2$a$) takes place, as discussed above, as $Y_i \to Y_{i,min}$. An interesting feature of these figures is that there appears to be a local minimum in the function $\tau_i(Y_i)$ at $Y_i \sim Y_{i,min}$.

## 4. Two-dimensional transient computations

The analysis in § 3 suggests that, for any displacement flow that leaves behind a static wall layer of fluid 2, the static layer thickness $h$ should not exceed $h_{max}$, within any essentially uni-directional region of flow. The analysis also leaves open the following three important questions:

(i) Although the interfaces in § 3.3 approach $h_{max}$ at large times, does $h_{max}$ predict the static residual layer thickness in more realistic displacement flows?

(ii) If a static wall layer is found, with thickness $h < h_{max}$, how is the thickness $h$ selected?

(iii) Do static wall layers always exist if $h_{max} > 0$?

In this section we present the results of a series of transient two-dimensional displacement computations, which begin to answer these questions. The computations take the form of a numerical experiment, in which fluid 2 is displaced by fluid 1, through a long slot. The displacement model is as in § 2.1. Details of the computational method are given immediately following. In § 4.1 we present example computations, we outline the principle differences between these displacements and the axial displacements in § 3.3 and we discuss the underlying structure of these displacement flows. Additionally, we make a number of comments about the appropriateness of our numerical method for computing displacements with static wall layers. Finally in § 4.2, we present results of a systematic comparison study of $h_{max}$ with the computed layer thickness $h$. This answers the first of the above questions.

*Computational details*

The following numerical experimental design was adopted for all computed results. We consider displacements through a half-slot: $(x, y) \in [0, 30] \times [0, 1]$. Flow symmetry is enforced via the conditions $u_y(x, 0, t) = 0$ and $v(x, 0, t) = 0$. No-slip conditions are satisfied at the wall, $y = 1$. The slot is initially filled with fluid 2, which is flowing steadily at a constant flow rate imposed via the inflow conditions of $u(0, y, t) = 1$ and $v(0, y, t) = 0$. This steady solution for fluid 2 is used as the initial condition for the displacement. At time $t = 0$, fluid 1 is injected at $x = 0$, also with uniform velocity $u(0, y, t) = 1$. This ensures compatibility of the initial conditions at the initial *interface* between the two fluids. For the parameters we have considered, the steady fluid-2 initial condition is found to settle to a classical Bingham–Poiseuille velocity profile only a few slot half-widths downstream from the inflow. We did not study entry-length specifically (but see Wilson & Taylor 1996), although this would be an interesting problem in its own right.

The computations were performed using the computational fluid dynamics (CFD) code FIDAP, version 8.01. This is a finite-element-based code and we have used a rectangular mesh with quadrilateral linear basis functions throughout. The mesh is refined towards the wall and towards the inflow. The effective viscosity of a true Bingham fluid becomes infinite in unyielded regions of the flow. Consequently, a viscosity regularization is necessary to model and compute visco-plastic fluid flows with CFD codes such as FIDAP. In this method, the constitutive laws are replaced by an effective-viscosity representation: $\tau_{k,ij} \equiv \eta_k \dot{\gamma}_{ij}$, where the effective viscosity $\eta_k$ is defined everywhere. We have used

$$\eta_k \equiv \mu_k + \frac{\tau_{k,Y}}{\dot{\gamma} + \epsilon}, \tag{4.1}$$

where $\epsilon$ is a numerical regularization parameter (also having a physical representation in terms of the limiting low-shear viscosity). Our choice is just one of many possible choices for $\eta_k$. Different meshes and regularizations were tested (the effective viscosity is implemented as a user-defined subroutine in FIDAP), and the results computed were found to be relatively robust with respect to small changes in either mesh size or viscosity regularization. The parameter $\epsilon = 10^{-3}$ was fixed throughout. We discuss the usage of regularized viscosity models such as (4.1) in § 4.1.2.

The displacement is handled using the volume-of-fluid (VOF) method. The discretization and implementation of the VOF method in FIDAP are both explained well in the Fidap 8 Theory Manual (1998). At base, the VOF method models the displacement as the advection of a passive scalar. Thus, in place of (2.16) a concentration $c(x, y, t)$ is advected:

$$\frac{\partial c}{\partial t} + u\frac{\partial c}{\partial x} + v\frac{\partial c}{\partial y} = 0, \tag{4.2}$$

with $c = 1$ in fluid 1 and $c = 0$ in fluid 2. At the *interface* there is a thin diffuse region of intermediate concentration in place of the sharp interface. A certain amount of numerical diffusion is inevitable in such computations, but the interfacial smearing is generally well controlled and remains confined to 1–2 mesh elements. In this method, intermediate concentration values are not coupled back into the momentum equations (e.g. via the definition of concentration-dependent density or rheology). Thus, apart from numerical diffusion, the advection of a passive scalar is modelled; cf. equations (2.13)–(2.18).

The computations were continued until $t = 25$, which corresponds to pumping $\frac{5}{6}$ of a slot volume. Small lengthwise variations in the computed residual layer thickness were often observed (see discussion in § 4.1.1). Thus, in order to estimate a representative residual layer thickness, $h(t)$ was defined by the following spatial average:

$$h(t) = 1 - \frac{1}{x_R - x_L}\int_0^1 \int_{x_L}^{x_R} c(x, y, t)\mathrm{d}x\mathrm{d}y, \tag{4.3}$$

where we have fixed $x_L = 15$ and $x_R = 25$. The layer thickness that we show in our computed results is always taken at $t = 25$, i.e. $h = h(t = 25)$. At $t = 25$, the front has passed the end of the averaging filter $x_R = 25$. The choice of $x_L = 15$, positions the beginning of the averaging filter well downstream of the inflow. Experience with a sequence of progressively longer filters showed that $x_R - x_L \approx 10$ was sufficiently large to average local variations.

When modelling a visco-plastic fluid with a regularized effective viscosity, such as (4.1), the fluid will always move under an applied stress, which would not be the case

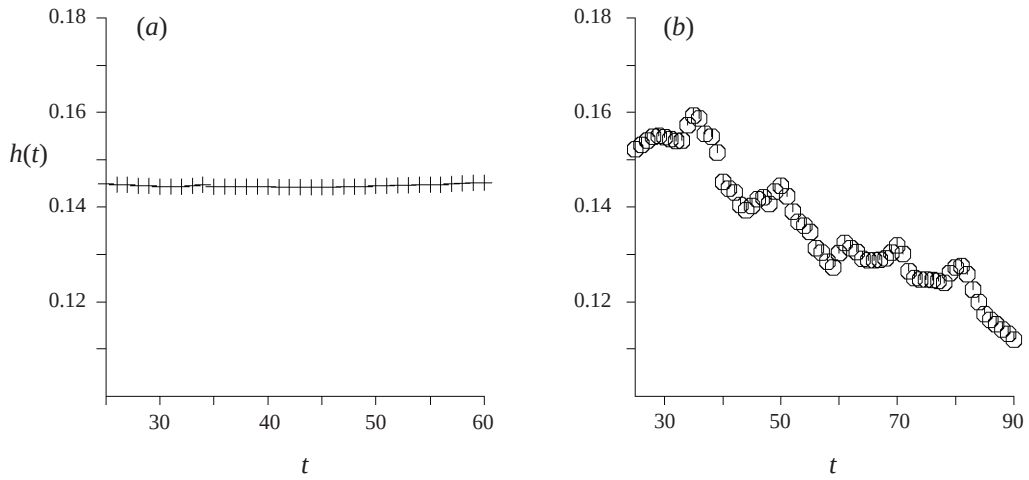


FIGURE 8. Example time evolution for static and transient $h(t)$:
$(a)$ $(\tau_{1,Y}, \tau_{2,Y}, \mu_1, \mu_2) = (0.2, 0.5, 0.01, 0.05)$; $(b)$ $(\tau_{1,Y}, \tau_{2,Y}, \mu_1, \mu_2) = (0.35, 0.5, 0.01, 0.05)$.

for an unyielded visco-plastic fluid adjacent to the wall. To distinguish layers that would be moving from those that would be static (i.e. if a true visco-plastic were flowing), we compute the shear stress $\tau_2(x, y, t)$ and the layer is considered truly static if

$$\tau_2 \leqslant \tau_{2,Y}. \tag{4.4}$$

The criterion (4.4) is not arbitrary. In place of a plastic yield limit we have simply a *very viscous* fluid. When $\tau_2 \sim \tau_{2,Y}$ then

$$\eta_k \sim \frac{\tau_{k,Y}}{\epsilon^{1/2}}, \tag{4.5}$$

and $\dot{\gamma} \sim \epsilon^{1/2}$. Thus, (4.4) will imply that $||\boldsymbol{u}|| = O(\epsilon^{1/2}h)$ for any layer close to the wall, and such layers will be effectively *static* for timescales less than $\sim \epsilon^{-1/2}h^{-1}$. This estimate is also conservative for $h < h_{max}$, since then $\tau_2 < \tau_{2,Y}$ throughout the wall layer and $\dot{\gamma}$ is smaller than $\sim \epsilon^{1/2}$. Furthermore, it is worth noting that for a static wall layer, the stress is largest at the wall, see figure 2($a$). Thus, $\dot{\gamma}$ decreases with distance from the wall. In practice, the difference between a static layer, satisfying (4.4), and one that is still evolving is quite obvious. Figure 8 shows an example of the time evolution of $h(t)$ for typical static and non-static layers.

### 4.1. *Example computations and displacement flow structure*

Two examples of iso-density displacement computations are shown in figures 9($a$) and 9($b$), where the dimensionless rheological parameters are: $(\tau_{1,Y}, \tau_{2,Y}, \mu_1, \mu_2) = (0.2, 0.5, 0.01, 0.05)$ and $(\tau_{1,Y}, \tau_{2,Y}, \mu_1, \mu_2) = (0.2, 1.0, 0.005, 0.01)$, respectively. The figures plot the concentration profiles at different times throughout the displacement computation. These dimensional parameters have been selected to enable direct comparison with the two axial displacement computations shown in figures 6 and 7. Before entering into detail, we draw attention to two principal differences between the fully two-dimensional displacement results and the axial displacement results in figures 6 and 7.

(i) The concentration profiles appear to propagate steadily along the slot, without changing shape. In the corresponding axial displacements, only the central part of

the interface propagates steadily (i.e. the shock). The rest of the interface in the axial displacement is *stretched out* behind the front and only asymptotically approaches $h_{max}$.

(ii) The residual wall layers in figures 9(*a*) and 9(*b*) have a thickness $h$ that is significantly less than the asymptotic residual wall layer thickness $h_{max}$, observed in figures 6 and 7.

In § 4.2 we explore the discrepancy between $h$ and $h_{max}$ in more detail and for a range of different dimensionless parameters. Here we explain the structure of the underlying steadily propagating displacement flow.

When fully steady and in a sufficiently long slot, the underlying structure of the displacement flow is as illustrated schematically in figure 10. There are three distinct regions. Downstream, sufficiently far ahead of the front, fluid 2 moves axially as a plane Bingham–Poiseuille flow with a plug region in the centre of the flow, as illustrated. Upstream, sufficiently far behind the displacement front, there will exist a two-layer flow. The axial velocity profile should be schematically as in figure 2(*a*), with one plug region attached to the wall and one plug region in the centre of the channel. Close to the displacement front there will exist a region where the flow is two-dimensional. The lengthscale of the two-dimensional frontal region is unknown, but appears to be only a few slot widths in our computations.

The frontal region is two-dimensional in two respects. First, the static layers that are upstream of the frontal region constrict the flow area. Thus, this region behaves as an expansion and the flow will be two-dimensional provided that the length of this region is not too long. Second, if we translate coordinates to a frame of reference that is moving with the constant speed of the displacement front, this frontal region will contain two-dimensional recirculatory zones for the translated velocity field (see later in § 5).

The transition between the axial flow regions and the frontal region is unclear. In particular, we have not studied the exact topology of the yield surfaces for the plug regions in the centre of the channel. Our numerical method is not fully suitable for such a study and ideally this type of numerical study should focus on a steady flow, which requires that the interface be specified.

Figure 11 shows results from one of our computations, close to the displacement front. In figure 11(*a*) the rate of strain $\dot{\gamma}$ is plotted. Below the lowest contour (the empty regions), we have $\tau_2 \leqslant \tau_{2,Y}$. We can see that the highest shear regions are concentrated, both upstream and downstream, in two shear layers that join one another in the frontal region. Apart from within this transitionary high shear layer, we have $\dot{\gamma} \sim O(1)$ throughout the frontal region. Additionally, there is a transitional region leading into the tip of the wall layer. From figure 11(*b*) we can see that the wall layer is not completely uniform. Figure 11(*c*) shows the streamlines for the flow, very clearly indicating the expansion effect and the near-axial regions of flow upstream and downstream.

#### 4.1.1. *Footprinting*

The irregular contours in the centre of figure 11(*a*), the uneven layering in figure 11(*b*) and the slight waviness of the streamlines in figure 11(*c*), all indicate that the displacement flow does not propagate absolutely steadily. Although the underlying steady propagation is believed to exist, the static layers are thought to be only marginally stable within the frontal region. The small (static) indentations that remain after the front has passed are believed to result from a *footprinting* mechanism, which we describe below.

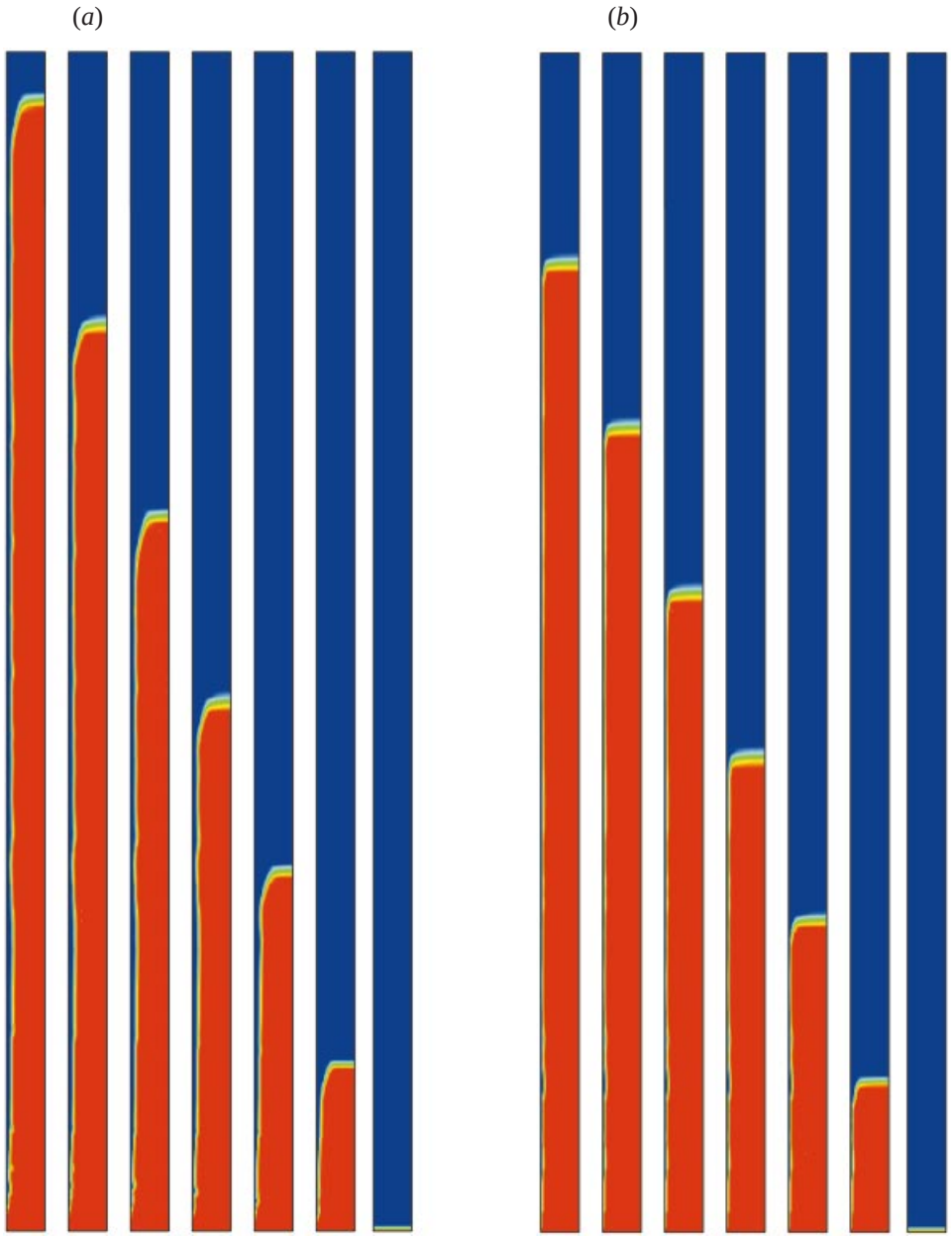


FIGURE 9. Two-dimensional iso-density displacements: $c(x, y, t) = 1$ is red, $c(x, y, t) = 0$ is blue. (*a*) Rheological parameters are $(\tau_{1,Y}, \tau_{2,Y}, \mu_1, \mu_2) = (0.2, 0.5, 0.01, 0.05)$; times (right to left): $t = 0.001, 3.8, 7.92, 11.7, 15.8, 20.0, 25.0$. (*b*) Rheological parameters are $(\tau_{1,Y}, \tau_{2,Y}, \mu_1, \mu_2) = (0.2, 1.0, 0.005, 0.01)$; times (right to left): $t = 0.001, 3.64, 7.54, 11.5, 15.4, 19.4, 23.4$.

For a true Bingham fluid, the residual wall layer is everywhere static and unyielded. After the displacement front has passed, if $h < h_{max}$, then the stresses in the static layer will be significantly below the yield stress of fluid 2. Thus, even small finite perturbations of the flow in the axial two-layer region should not affect the static layer thickness, i.e. the layers in this region should be stable. Conversely, this also

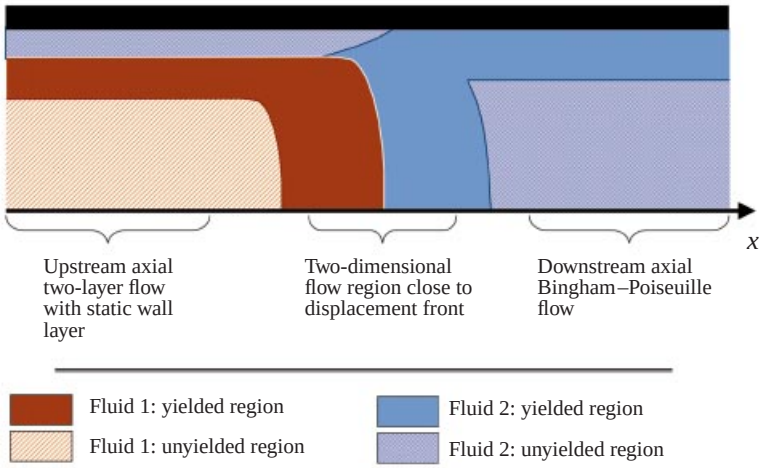


FIGURE 10. Schematic of the displacement flow structure for a fully steady two-dimensional displacement leaving behind a static wall layer.

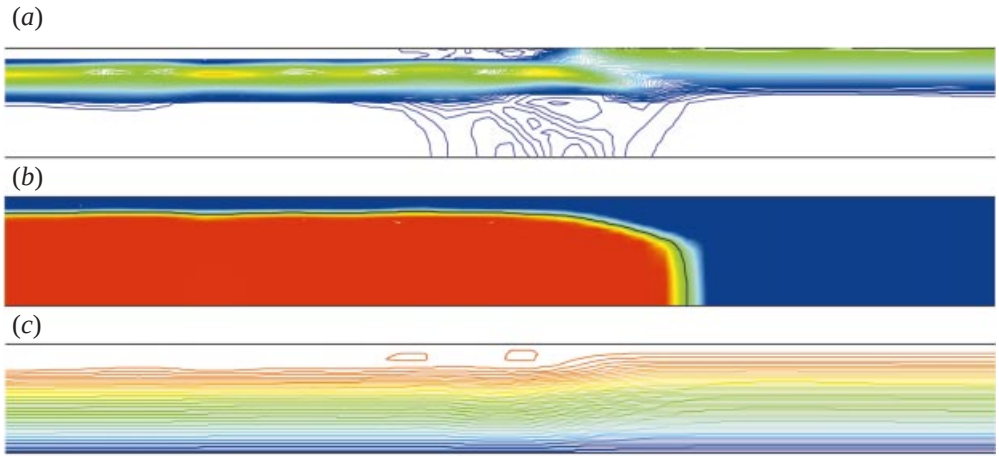


FIGURE 11. Results of a transient two-dimensional iso-density displacement, close to the displacement front: (*a*) contours of $\dot{\gamma}$, spaced at intervals $\Delta\dot{\gamma} = 0.1$; (*b*) fluid concentration, $c(x, y, t) = 1$ is red, $c(x, y, t) = 0$ is blue; (*c*) streamlines with spacing $\Delta\Psi = 0.02$. Rheological parameters are $(\tau_{1,Y}, \tau_{2,Y}, \mu_1, \mu_2) = (0.2, 0.5, 0.01, 0.05)$ and the fixed time is $t = 15.8$.

means that any slight non-uniformity or indentation in the static layer can remain there indefinitely, i.e. it can be footprinted into the layer.

Downstream from the displacement front, fluid 2 is yielded at the wall. Upstream, fluid 2 is unyielded. By continuity therefore, there will exist a point on the wall at which the wall stress is equal to the yield stress. The yield surface emanating from this point forms the boundary of the static residual layer and eventually will curve to join the interface at some point upstream, behind the propagating displacement front, see figure 10. This yield surface is therefore located close to the displacement front, in the region of flow that is two-dimensional. Unlike upstream, in this region any infinitesimal perturbation in the stress field is able to perturb the surface of the static layer. In this sense, we believe that the idealized state of a steady and uniform static layer being left behind a displacement flow is only marginally stable.

Note that an initial deviation from the idealized state of a steady and uniform static layer displacement flow is provided in our simulations by the inflow condition. Displacement front instabilities may also occur at moderate Reynolds numbers due to hydrodynamic effects (e.g. symmetry breaking in channel expansions). Numerical errors are also ever present. We have not studied any of these possibilities in detail, but believe that the slight flow unsteadiness and layer non-uniformity can be explained in this way. Interestingly, a sufficiently large indentation in the static layer might result in the generation of shear stress perturbations sufficient to remove the static layers. We note that the footprinting mechanism that we describe is completely analogous to the pressure-pulse footprinting that is described in Liu & Mei (1989), who consider the free-surface flow of a Bingham fluid down an incline.

4.1.2. *Using effective-viscosity regularizations for visco-plastic fluid flows*

We are cautious in using an effective-viscosity regularization such as (4.1). Such regularizations have become commonplace in recent years and represent the simplest way to compute visco-plastic fluid flows, by using the structure of existing CFD codes. Justification for the use of regularization methods is rarely given and we know of no rigorous results for transient inertial displacement flows, as here. The effectiveness of the method for our computations is therefore inferred from results that are valid for simpler problems.

Considering slow internal flows of a single Bingham fluid, the primary justification for using (smooth) regularizations such as (4.1) rests on being able to prove convergence of the regularized solution, say $\boldsymbol{u}_\epsilon$, to the true solution $\boldsymbol{u}$, as $\epsilon \to 0$, in an appropriate norm. An example of how to do this can be found in Glowinski (1983, p. 83). As with many regularization methods, the limit $\epsilon \to 0$ nearly always leads to numerically ill-conditioned problems on implementation. Thus, most practical usage involves a small fixed $\epsilon$, balancing the requirement of theoretical convergence to the true Bingham fluid velocity field with computational convergence.

What methods, such as that of Glowinski, do not establish is the convergence of the two deviatoric stress tensors as $\epsilon \to 0$. The reason here is straightforward, namely that the stresses are indeterminate for a true Bingham fluid in all regions where the fluid is unyielded, but are determined everywhere if a regularized viscosity model is used, i.e. there need not be convergence of the deviatoric stress tensors. The uncertainty of using a viscosity regularization such as (4.1) is thus focused specifically on predicting the positions of yield surfaces and knowing whether computed regions of low-shear flow would in fact be unyielded had the true constitutive laws (2.17) and (2.18) been used. An interesting and very under-utilized result, which can help here, is the stress minimization principle of Prager (1954). This result often implies that, of all admissible stress tensors, the deviatoric stress tensor of the Bingham fluid is that which is least likely to yield. Hence, in situations when the stress tensor corresponding to (4.1) is admissible, flow regions where $\tau_k \leqslant \tau_{k,Y}$ is computed can be considered as unyielded for the true Bingham fluid rheology. This gives a one-sided bound at least.

Clearly, whether or not effective viscosity regularization is a viable computational method is problem-dependent. If the goal is simply to determine the velocity field, then effective-viscosity regularization is usually viable. When this is not the case, the chief problem in using (4.1) becomes one of interpretation. The theoretical convergence results give $||\boldsymbol{u} - \boldsymbol{u}_\epsilon|| \sim \delta(\epsilon)$, where $\delta(\epsilon) = o(\epsilon)$, and the convergence norm is typically $H^1$. Thus, wherever $\dot{\gamma}(\boldsymbol{u}_\epsilon) \gg \delta(\epsilon)$, we expect that the deviatoric stresses also converge, i.e. in those regions where the true Bingham fluid stresses are determinate. Similarly, small $\dot{\gamma}(\boldsymbol{u}_\epsilon)$ will be found in the same regions of flow as for the true Bingham fluid.

However, in regions where $\dot{\gamma}(\boldsymbol{u})$ is small, a true Bingham fluid can have both *true plug* (i.e. unyielded) and *pseudo-plug* regions. Without further analysis, it is often difficult to distinguish between true plug and pseudo-plug regions for results computed using an effective-viscosity regularization. Good examples of true and pseudo-plug behaviour are given in Szabo & Hassager (1992), Walton & Bittleston (1991) and Wilson (1993*a*, *b*).

We turn specifically now to our problem, which is inertial, fully transient and two-fluid. We first remark that the inertial terms are not dominant for the dimensionless parameter values that we have used, as is evidenced by the steadily propagating computed displacements. If $||\boldsymbol{u} - \boldsymbol{u}_\epsilon|| \sim o(\epsilon)$ were valid for the analogous steady problem, as effectively we assume, then we must expect that this will hold for the transient problem only over time intervals $\Delta t = O(1)$ (i.e. viewing (4.1) purely as a perturbation method); hence the finite simulation time $t = 25$. As regards having multiple fluids, we comment only that both fluids are yielded close to the advancing displacement front, where the flow is two-dimensional. We can therefore expect that the stresses and velocities, computed from the regularized model (4.1), will be close to those of the true Bingham model in this region. Insofar as the velocities and stresses in this region are believed to determine the layer thickness, we believe our computations, based on (4.1), to be reasonable. However, as pointed out above, there could still be problems in interpreting certain regions of low shear that we compute.

We consider first the upstream wall layers. Suppose the fluid-2 residual layer has thickness $h < h_{max}$. Once the displacement front has passed, the flow is observed to become near-axial. If we now compute the corresponding axial two-layer velocity profile (for a true Bingham fluid), this velocity profile will have a plug region at the wall, throughout fluid 2, and a second plug region in the middle of the fluid-1 layer, e.g. see figure 2(*a*). Due to the no-slip condition, each plug predicted at the wall has zero velocity. Thus, no extensional rate of strain exists in the wall layer and we can expect that the axial shear flow scaling remains valid throughout the static wall layer, i.e. a static wall layer is truly static for a true Bingham fluid. Interpreting the two unattached plug regions that are shown schematically in figure 10, in the mid-channel, is much harder. Either could consist of true plug regions and/or pseudo-plug regions. Probably, downstream the fluid-2 plug will be a true plug, with only a pseudo-plug possible in the transition to the frontal region. Upstream, if the footprinting mechanism results in a slowly varying static wall layer thickness (i.e. for a physical reason, not a numerical reason), then the plug will almost certainly consist of true plug and pseudo-plug regions, also with a possible transitional pseudo-plug in the transition to the frontal region.

It is clear that if we wish to study the topological behaviour of the yield surfaces in the channel centre, the method we have used is not viable. However, since the interface, denoting the boundary of the static wall layer with fluid 1, is not a yield surface, the method appears to be quite adequate for predicting the residual layer thickness, and it is purely for this purpose that it is used.

### 4.2. *Parametric variations in the layer thickness*

In order to make a direct comparison between the computed residual layer $h$ and $h_{max}$, two series of computations have been carried out. The first series of computations is based on the parameters

$$(\tau_{1,Y}, \tau_{2,Y}, \mu_1, \mu_2) = (0.2, 0.5, 0.01, 0.05)$$

(see figure 9*a*) with variations in each of the four rheological parameters being examined separately. The second series of computations is analogous, but centred on

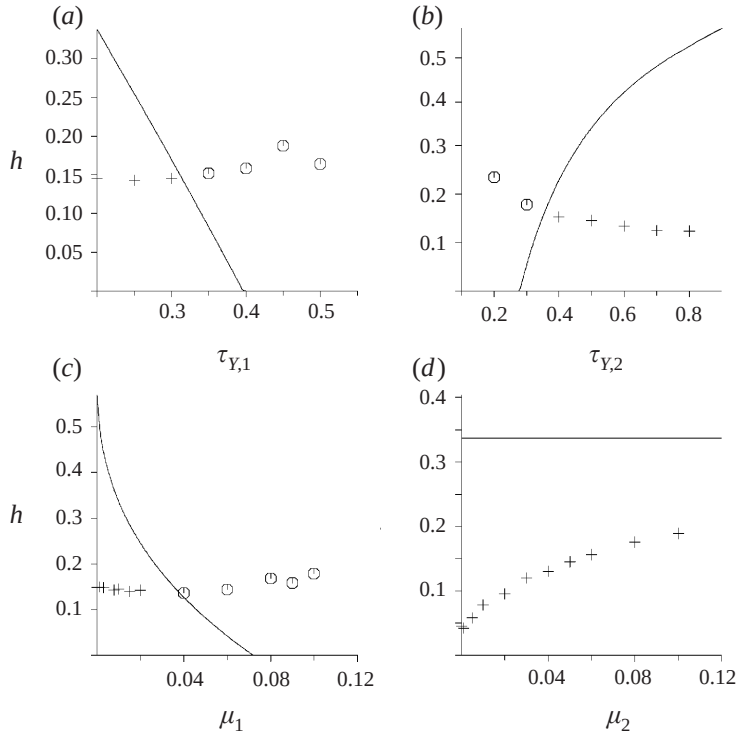


FIGURE 12. Comparisons of $h$ (symbols) and $h_{max}$ for iso-density displacements. Parametric variation centred about $(\tau_{1,Y}, \tau_{2,Y}, \mu_1, \mu_2) = (0.2, 0.5, 0.01, 0.05)$: (*a*) variation with $\tau_{1,Y}$; (*b*) variation with $\tau_{2,Y}$; (*c*) variation with $\mu_1$; (*d*) variation with $\mu_2$. Points marked with a circle are transient layers, those marked with a cross are static.

the parameters

$$(\tau_{1,Y}, \tau_{2,Y}, \mu_1, \mu_2) = (0.2, 1.0, 0.005, 0.01)$$

(see figure 9*b*). These two comparisons are plotted in figures 12 and 13.

The results plotted in figures 12 and 13 are qualitatively similar, suggesting consistency, but are also quite surprising. The variation of $h$ with the parameters $\tau_{1,Y}$, $\tau_{2,Y}$ and $\mu_1$ appears to be almost opposite to that of $h_{max}$. Intuitively, one might expect that the residual layer thickness would increase with the yield stress of the displaced fluid $\tau_{2,Y}$, but this is not the observed effect. Although $h_{max}$ is not a direct prediction of the layer thickness, it appears to vary with $\tau_{2,Y}$ in the way that is physically intuitive. Similarly, physical intuition suggests that increases in either $\tau_{1,Y}$ or $\mu_1$ should decrease the residual layer thickness. Although $h_{max}$ decreases with these parameters, $h$ is constant, or even slightly increasing. In contrast, physical intuition would predict that $h$ increases with $\mu_2$, and this is indeed observed, whereas the determination of $h_{max}$ is independent of $\mu_2$. Where $h_{max}$ does give a good prediction is in dividing the layers that are transient $h > h_{max}$, from those that are static $h < h_{max}$.

### 4.2.1. *Simple explanation for* $h < h_{max}$

That static residual layers $h$, computed from a fully two-dimensional model, should be less than $h_{max}$ is to be expected. The fully two-dimensional flow is likely to generate higher stresses at the displacement front than those in an axial flow with the same interface position. Since the definition of $h_{max}$ considers an axial flow in which the yield stress is attained exactly at the wall, any displacement flow that generates larger stresses is likely to leave only static layers $h < h_{max}$.

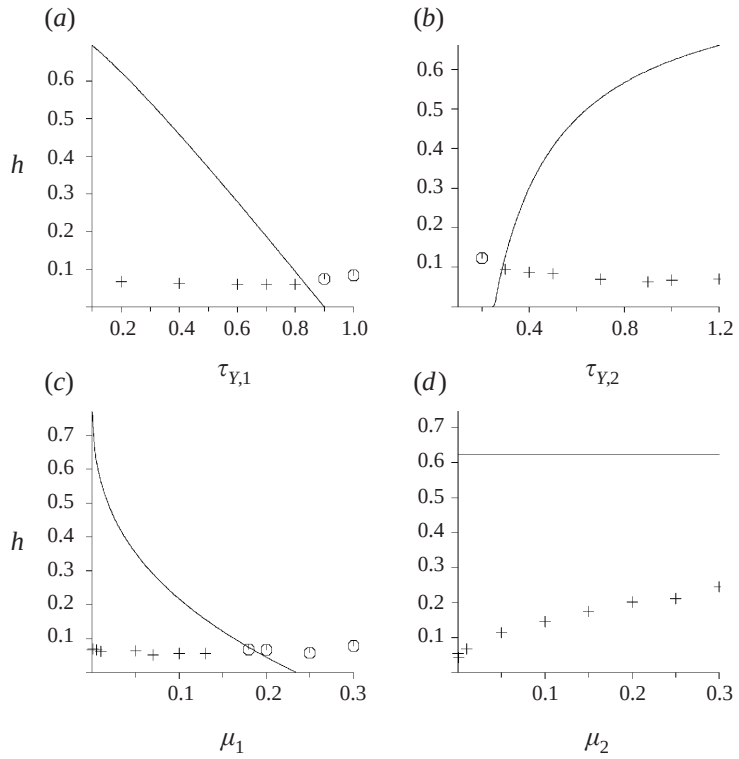


FIGURE 13. Comparisons of $h$ and $h_{max}$ for iso-density displacements. Parametric variation centred about $(\tau_{1,Y}, \tau_{2,Y}, \mu_1, \mu_2) = (0.2, 1.0, 0.005, 0.01)$: (*a*) variation with $\tau_{1,Y}$; (*b*) variation with $\tau_{2,Y}$; (*c*) variation with $\mu_1$; (*d*) variation with $\mu_2$. Points marked with a circle are transient layers, those marked with a cross are static.

## 5. Steady two-dimensional displacements and static layer thickness selection

It is evident from the large discrepancy between computed $h$ and $h_{max}$, in § 4.2, that the two-layer axial model is far too simplistic to be able predict the static layer thickness $h$. The results in § 4 also suggest that these transient displacements are characterized by an underlying steadily propagating two-dimensional displacement flow, which leaves behind a uniform static wall layer. We turn now to an analysis of this basic steady flow in the hope of better understanding the selection of static wall layer thickness.

We succeed in offering a simple prediction of static layer thickness that is in good agreement with the computed results of § 4. This prediction is based on the notion of a limiting static layer thickness, which approximately minimizes the rate of visco-plastic dissipation local to the displacement front. It is argued heuristically that this limiting layer thickness will be close to the limiting layer thickness, $h_{circ}$, at which the streamlines in fluid 2 begin to recirculate ahead of the displacement front, when viewed in a steadily advancing frame of reference. In § 5.1 we introduce the steady-state displacement model. In § 5.2 we show that fluid 2 will recirculate for uniform static layers $h < h_{circ}$, we compare the results of § 4.2 with parametric variations in $h_{circ}$, and we explain why this limit should approximately minimize the local rate of dissipation.

### 5.1. *Steady-state displacement model*

We suppose dimensionless parameters such that $h_{max} > 0$ and suppose that the displacement profile propagates steadily with a speed $S$ in the positive $x$-direction, leaving behind a uniform static wall layer. Both the interface and velocity field remain steady in a frame reference moving with the displacement front. Writing $X = x - St$, $Y = y$, $U = u - S$, $V = v$ and $P = p + x/F$, the steady equations of motion become

$$r\left[U\frac{\partial U}{\partial X} + V\frac{\partial U}{\partial Y}\right] = -\frac{\partial P}{\partial X} + \frac{\partial}{\partial X}\tau_{1,XX} + \frac{\partial}{\partial Y}\tau_{1,XY} - b, \quad (X,Y) \in \Omega_1, \tag{5.1}$$

$$r\left[U\frac{\partial V}{\partial X} + V\frac{\partial V}{\partial Y}\right] = -\frac{\partial P}{\partial Y} + \frac{\partial}{\partial X}\tau_{1,YX} + \frac{\partial}{\partial Y}\tau_{1,YY}, \quad (X,Y) \in \Omega_1, \tag{5.2}$$

$$U\frac{\partial U}{\partial X} + V\frac{\partial U}{\partial Y} = -\frac{\partial P}{\partial X} + \frac{\partial}{\partial X}\tau_{2,XX} + \frac{\partial}{\partial Y}\tau_{2,XY}, \quad (X,Y) \in \Omega_2, \tag{5.3}$$

$$U\frac{\partial V}{\partial X} + V\frac{\partial V}{\partial Y} = -\frac{\partial P}{\partial Y} + \frac{\partial}{\partial X}\tau_{2,YX} + \frac{\partial}{\partial Y}\tau_{2,YY}, \quad (X,Y) \in \Omega_2, \tag{5.4}$$

$$0 = \frac{\partial U}{\partial X} + \frac{\partial V}{\partial Y}, \quad (X,Y) \in \Omega_k, \quad k = 1,2, \tag{5.5}$$

where $\Omega_k$ denotes the region occupied by fluid $k$. Both rate of strain and shear stress definitions are unchanged by the coordinate transformation; the constitutive equations remain (2.17) and (2.18).

The length of the domain in the $X$-direction is taken to be $X \in [-L, L]$, where $L$ is considered sufficiently large for the flow to become axial at $X = \pm L$. The fluid domains and flow structure are assumed to be schematically as in figure 10. Thus, $Y_i(X) = 0$ for $X \geqslant 0$ and $Y_i(X) > 0$ for $X < 0$. Only uniform static layer thicknesses $h \in (0, h_{max})$ are considered. Therefore, upstream at $X = -L$, $Y_i(X) = Y_{-L} \in (Y_{i,min}, 1)$. Furthermore, since we consider properly steady propagation, the interface $Y = Y_i(X)$ is assumed to become parallel to the wall some distance before $X = -L$. The kinematic equation for the interface is

$$U\frac{\partial Y_i(X)}{\partial X} = V, \tag{5.6}$$

from which it follows that the interface is a streamline for the steady flow.

#### 5.1.1. *Boundary conditions*

Boundary conditions for the transformed velocity on $Y = 0$ and $Y = 1$ are

$$V(X,0) = 0, \tag{5.7}$$

$$\tau_{k,XY}(X,0) = 0 \Longrightarrow \frac{\partial U}{\partial Y}(X,0) = 0, \tag{5.8}$$

$$U(X,1) = -S, \tag{5.9}$$

$$V(X,1) = 0. \tag{5.10}$$

The downstream boundary condition is that of a plane Bingham–Poiseuille flow of fluid 2, translated by the mean propagation speed, i.e.

$$U(L,Y) = U_L(Y), \quad V(L,Y) = 0, \tag{5.11}$$

where

$$U_L(Y) = \begin{cases} \dfrac{3}{Y_{2,Y}+2} - S, & Y \in [0, Y_{2,Y}) \\ \dfrac{3}{Y_{2,Y}+2}\left[1 - \dfrac{(Y-Y_{2,Y})^2}{(1-Y_{2,Y})^2}\right] - S, & Y \in [Y_{2,Y}, 1], \end{cases} \tag{5.12}$$

where $Y = Y_{2,Y}$ is the position of the yield surface. This position is given by

$$Y_{2,Y} = \frac{1}{\xi(B_2)}, \tag{5.13}$$

where $\xi(B_2) > 1$ is the root of the parametric cubic equation (3.24) (see § 3.2). $B_2$ is the Bingham number of fluid 2:

$$B_2 = \frac{\tau_{2,Y}}{\mu_2} = \frac{\hat{\tau}_{2,Y}\hat{D}}{\hat{\mu}_2\hat{U}_0}. \tag{5.14}$$

Note from (5.12) that

$$\int_0^1 U_L(Y)\mathrm{d}Y = 1 - S, \tag{5.15}$$

which is the transformed version of the flow rate constraint (3.10).

Upstream, the inflow is an axial flow with a static wall layer (e.g. figure 2*a*), translated by the mean propagation speed, i.e.

$$U(-L, Y) = U_{-L}(Y), \quad V(-L, Y) = 0, \tag{5.16}$$

where

$$U_{-L}(Y) = \begin{cases} \dfrac{3}{Y_{1,Y}+2Y_{-L}} - S, & Y \in [0, Y_{1,Y}) \\ \dfrac{3}{Y_{1,Y}+2Y_{-L}}\left[1 - \dfrac{(Y-Y_{1,Y})^2}{(Y_{-L}-Y_{1,Y})^2}\right] - S, & Y \in [Y_{1,Y}, Y_{-L}] \\ -S, & Y \in (Y_{-L}, 1], \end{cases} \tag{5.17}$$

where $Y = Y_{1,Y}$ is the position of the yield surface in fluid 1. This position is given by

$$Y_{1,Y} = \frac{Y_{-L}}{\xi(\tilde{B}_1)}. \tag{5.18}$$

Note from (5.17) that

$$\int_0^1 U_{-L}(Y)\mathrm{d}Y = 1 - S. \tag{5.19}$$

5.1.2. *Stream-function formulation*

For the remainder of this paper we are concerned solely with the generic behaviour of the streamlines. We define the stream function $\Psi(X, Y)$ in the usual way:

$$\Psi(X, Y) \equiv \int_{(0,0)}^{(X,Y)} U\mathrm{d}Y - V\mathrm{d}X. \tag{5.20}$$

Equations (5.1)–(5.5) can be reduced to a single fourth-order equation for the stream function, valid within each fluid domain $\Omega_k$:

$$r_k[\Psi_Y(\nabla^2\Psi)_X - \Psi_X(\nabla^2\Psi)_Y] = \left[\frac{\partial^2}{\partial Y^2} - \frac{\partial^2}{\partial X^2}\right]\tau_{k,XY} + 2\frac{\partial^2}{\partial X\partial Y}\tau_{k,XX}. \tag{5.21}$$

Note that $\tau_{k,XX} = -\tau_{k,YY}$, $\tau_{k,XY} = \tau_{k,YX}$, $r_1 = r$, $r_2 = 1$, and the constitutive equations need to be rewritten in terms of the second partial derivatives of the stream function, but this is a purely algebraic task.

The boundary conditions for $\Psi$ at inflow and outflow are

$$\Psi(\pm L, Y) = \Psi_{\pm L}(Y) \equiv \int_0^Y U_{\pm L}(Y)\mathrm{d}Y, \tag{5.22}$$

$$\Psi_X(\pm L, Y) = 0. \tag{5.23}$$

Boundary conditions for $\Psi$ at the wall are

$$\Psi(X,1) = 1 - S, \quad \Psi_Y(X,1) = 0, \tag{5.24}$$

and on the slot centreline

$$\Psi(X,0) = 0, \quad \Psi_{YY}(X,0) = 0. \tag{5.25}$$

Across the interface, both $\Psi$ and its normal derivative are continuous. Since the interface intercepts the $X$-axis at $X = 0$, it is clear that

$$\Psi(X, Y_i(X)) = 0. \tag{5.26}$$

Therefore, as well as (5.19), we have that

$$\int_0^{Y_{-L}} U_{-L}(Y)\mathrm{d}Y = 0. \tag{5.27}$$

Combining (5.19) and (5.27) with the fact that $U_{-L}(Y) = -S$ for $Y \in [Y_{-L}, 1]$ leads to

$$\int_{Y_{-L}}^1 U_{-L}(Y)\mathrm{d}Y = -S[1 - Y_{-L}] = 1 - S \Longrightarrow S \equiv \frac{1}{Y_{-L}}. \tag{5.28}$$

Equation (5.28) expresses the simple kinematic relationship between the width of a steadily propagating displacement finger and the speed of propagation.

### 5.2. *Generic streamline behaviour and $h_{circ}$*

Equation (5.27) effectively says that, whatever flows in at $X = -L$ for $Y \in (0, Y_i)$ must also flow out. Consequently, the fluid-1 streamlines are always recirculating in $\Omega_1$. At the inflow, from (5.17) and (5.28) it can be seen that $U_{-L}(0) > 0$, $U_{-L}(Y_{-L}) < 0$ and $U_{-L}(Y)$ is decreasing in $[0, Y_{-L}]$. Thus, there is a single zero of $U_{-L}(Y)$ in $[0, Y_{-L}]$ and a single maximum of $\Psi_{-L}(Y)$ in $[0, Y_{-L}]$. The fluid-1 streamlines enter $\Omega_1$ along the interval $[0, Y_{-L,zero})$ and exit $\Omega_1$ along the interval $(Y_{-L,zero}, Y_{-L}]$, where $Y_{-L,zero}$ is the single zero of $U_{-L}(Y)$. Note also that for $Y \in [0, Y_{1,Y}]$, fluid 1 is unyielded and the stream-function is simply given by $\Psi_{-L}(Y) = Y\,U_{-L}(0)$. The fluid-2 streamlines at the inflow are parallel and are uniformly spaced within the static wall layer, i.e. $\Psi(X,Y) = 1 - SY$ for $Y \in (Y_{-L}, 1]$.

At the outflow, from (5.12) we can see that $U_L(Y)$ is decreasing for $Y \in [0,1]$, and strictly decreasing for $Y \in (Y_{2,Y}, 1]$. Thus, $U_L(Y)$ has a single zero if and only if $U_L(0) > 0$. If $U_L(0) < 0$, then there are no zeros, and if $U_L(0) = 0$, then there are zeros $\forall\, Y \in (Y_{2,Y}, 1]$. We consider these two principal cases separately.

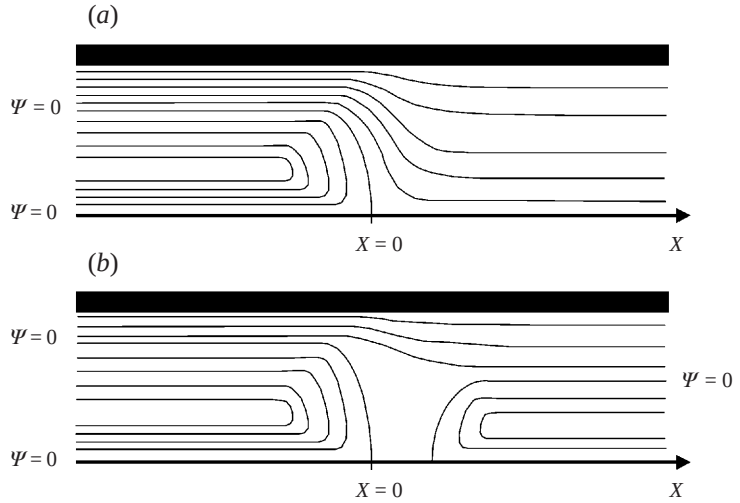


FIGURE 14. Schematic illustration of the two types of streamline behaviour: (*a*) no recirculation in fluid 2; (*b*) with recirculation in fluid 2.

(i) $U_L(0) < 0$: Since $\Psi_L(0) = 0$ and $\Psi_L(1) = 1-S < 0$, this implies that $\Psi_L(Y) < 0$, $\forall\, Y \in [0,1]$. In this case there are no zeros of $\Psi_L(Y)$ for $Y \in [0,1]$. The streamlines that enter $\Omega_2$ at $X = L$ for $Y \in (0,1)$ will exit $\Omega_2$ at $X = -L$ for $Y \in (Y_{-L}, 1)$, through the static layer.

(ii) $U_L(0) > 0$: In this case, $\Psi_L(Y) > 0$ in a neighbourhood of $Y = 0$, and $\Psi_L(Y)$ has exactly one zero for $Y \in [0,1]$, say $Y = Y_{L,zero}$. The streamline $\Psi = 0$ that enters $\Omega_2$ at $X = L$ and $Y = Y_{L,zero}$ cannot exit $\Omega_2$ at $X = -L$ or at $Y = 1$, since the boundary conditions there prevent $\Psi = 0$. The only possibilities now are that the streamline terminates either by intercepting the interface, creating a saddle point (thought to be unlikely in a steady propagation), or intercepts the slot centreline. In either case, this zero streamline will divide $\Omega_2$ into two distinct regions. The fluid-2 streamlines that enter $\Omega_2$ at $X = L$ for $Y \in (Y_{L,zero}, 1]$, will exit $\Omega_2$ at $X = -L$ for $Y \in (Y_{-L}, 1]$, through the static layer. The streamlines that enter $\Omega_2$ at $X = L$ for $Y \in [0, Y_{L,zero})$ must also exit $\Omega_2$ at $X = -L$ in this same interval. Since $\Psi_L(Y)$ will have a single maximum for $Y \in [0, Y_{L,zero})$, there will be a recirculation zone in fluid 2.

Assuming that neither fluid recirculates unnecessarily, there will be just two qualitatively different patterns of the streamlines, which we illustrate schematically in figure 14. In making this statement, we ignore the marginal state when $U_L(0) = 0$.

From (5.12) we see that $U_L(Y)$ depends upon $Y_{2,Y}$ (which is a function only of $B_2$), and on the propagation speed $S$, which is defined in terms of the static layer thickness by (5.28). Thus, the marginal state $U_L(0) = 0$, which delineates the two different streamline behaviours shown in figure 14, also defines a critical layer thickness $h_{circ}$ that controls streamline recirculation in fluid 2. For static layers that are thinner than $h_{circ}$, fluid 2 will recirculate. It is easily seen that

$$h_{circ}(B_2) = \frac{\xi(B_2) - 1}{3\xi(B_2)}, \tag{5.29}$$

which is sketched in figure 15. Figure 16 shows examples of inflow and outflow stream functions and velocities, for values of $h$ slightly above and below $h_{circ}$, with rheological parameters $(\tau_{1,Y}, \tau_{2,Y}, \mu_1, \mu_2) = (0.2, 0.5, 0.01, 0.05)$.

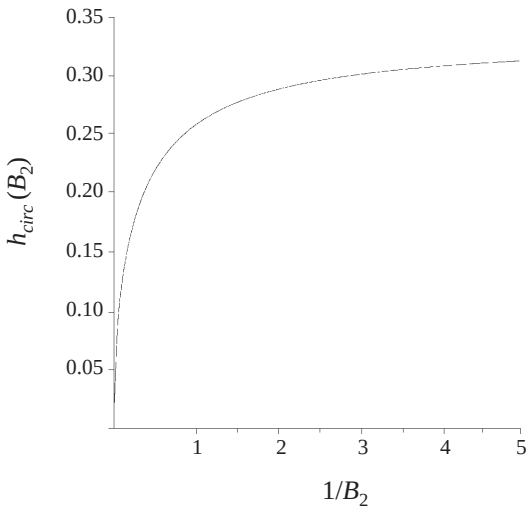


FIGURE 15. The function $h_{circ}(B_2)$, plotted against $1/B_2$.

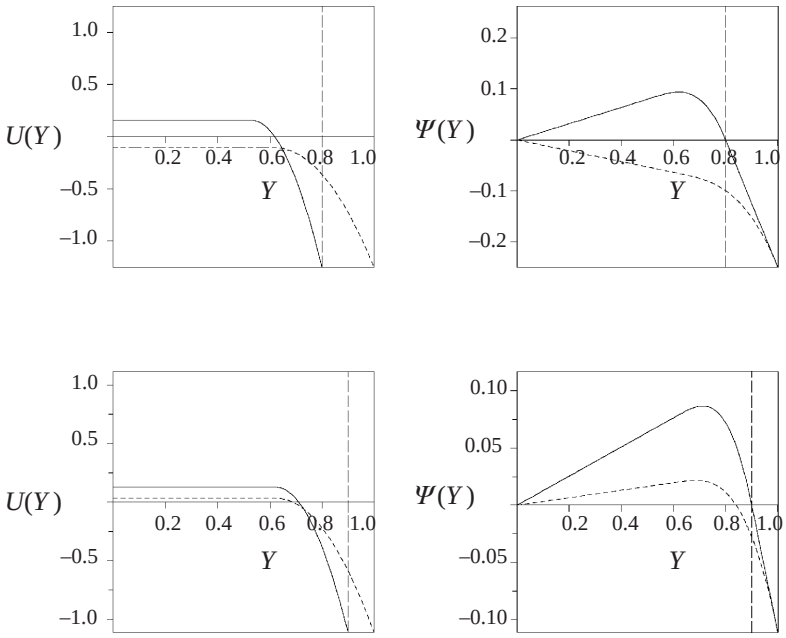


FIGURE 16. The functions $\Psi_{\pm L}(Y)$, $U_{\pm L}(Y)$ $(\tau_{1,Y}, \tau_{2,Y}, \mu_1, \mu_2) = (0.2, 0.5, 0.01, 0.05)$. Top figures: $h = 0.2$ (no recirculation); bottom figures $h = 0.1$ (recirculation). $\Psi_L(Y)$ and $U_L(Y)$ are marked with the dashed line. Vertical line denotes the interface.

### 5.2.1. *Comparisons of $h_{circ}$ with $h$*

In figures 17 and 18 we have plotted the parametric variation of $h_{circ}$ against each of the parameters $\tau_{1,Y}$, $\tau_{2,Y}$, $\mu_1$ and $\mu_2$ for the same ranges as in figures 12 and 13. We also compare with the computed values of $h$, from § 4.2. For those $h$ that are static, the agreement is very good. Not only does $h_{circ}$ give a good quantitative prediction of static $h$, but also the parametric variations in $h$ are predicted remarkably well.

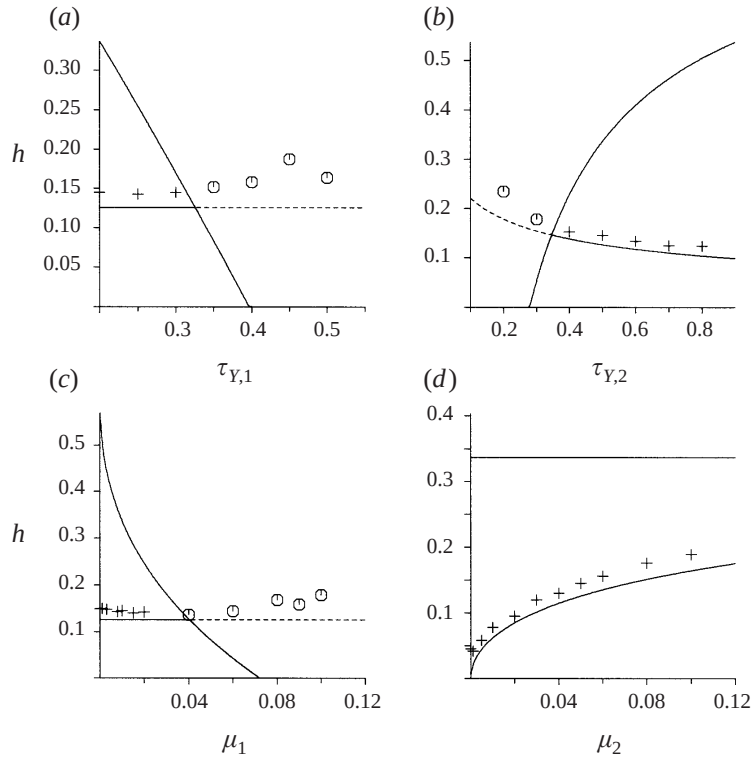


FIGURE 17. Comparisons of $h$ and $h_{circ}$ for iso-density displacements. Parametric variation centred about $(\tau_{1,Y}, \tau_{2,Y}, \mu_1, \mu_2) = (0.2, 0.5, 0.01, 0.05)$: (*a*) variation with $\tau_{1,Y}$; (*b*) variation with $\tau_{2,Y}$; (*c*) variation with $\mu_1$; (*d*) variation with $\mu_2$. Dashed line for $h_{circ} > h_{max}$. Points marked with a circle are transient layers, those marked with a cross are static.

### 5.2.2. *An heuristic physical explanation for* $h_{circ} \approx h$

We are unable to explain precisely why $h_{circ}$ should give such a good prediction of the static layer thickness. However, the following heuristic physical explanation is believed to be essentially correct.

First of all, note that for the parameters considered, the plastic viscosities $\mu_k$ are generally small but the yield stresses $\tau_{k,Y}$ are not small. The velocities are $\sim 1$, due to the scaling, and rates of strain are consequently $O(1)$. This means that the effective viscosities in yielded regions are typically $\sim \tau_{k,Y}$. Consequently, Reynolds numbers can be interpreted as having size $\sim 1/\tau_{k,Y}$ in the displacements computed. Thus, although not strictly slow, inertial effects are probably not particularly important in significant regions of the flow (although included for completeness).

If the flow is essentially non-inertial, we hypothesize that the displacement front configures itself locally to minimize the visco-plastic dissipation rate functional $D(\boldsymbol{U})$, close to the displacement front, i.e.

$$D(\boldsymbol{U}) = \sum_{k=1,2} \int_{\Omega_{l,k}} \mu_k \dot{\gamma}^2(\boldsymbol{U}) + \tau_{k,Y} \dot{\gamma}(\boldsymbol{U}) \mathrm{d}\Omega, \tag{5.30}$$

where $\Omega_{l,k} = \Omega_k \bigcap [-l, l] \times [0, 1]$ and the flow becomes axial outside of $X \in [-l, l]$. Note that the far-field flows are in equilibrium. For any parallel static layer at large

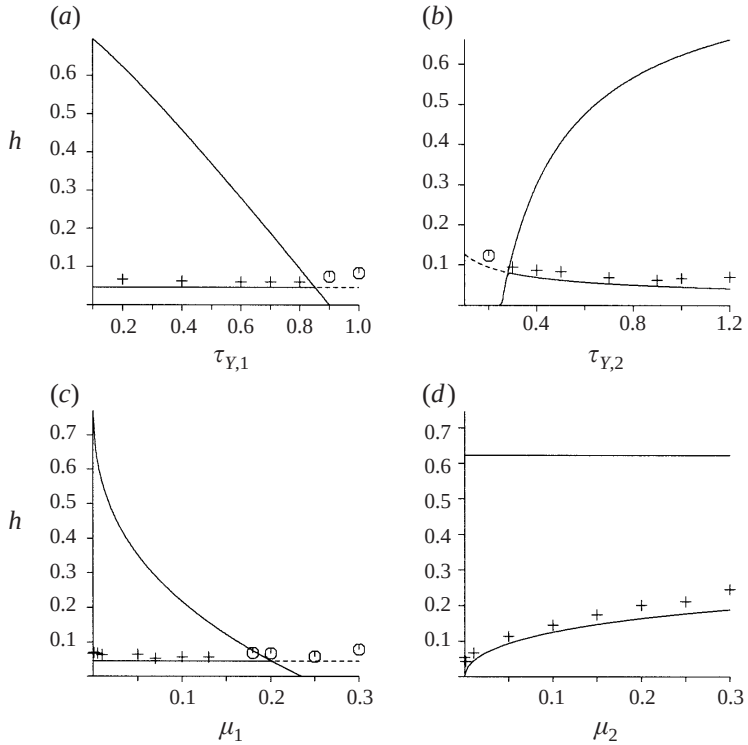


FIGURE 18. Comparisons of $h$ and $h_{circ}$ for iso-density displacements. Parametric variation centred about $(\tau_{1,Y}, \tau_{2,Y}, \mu_1, \mu_2) = (0.2, 1.0, 0.005, 0.01)$: (*a*) variation with $\tau_{1,Y}$; (*b*) variation with $\tau_{2,Y}$; (*c*) variation with $\mu_1$; (*d*) variation with $\mu_2$. Dashed line for $h_{circ} > h_{max}$. Points marked with a circle are transient layers, those marked with a cross are static.

negative $X$, the far-field energy equation for (5.1)–(5.5) is equivalent to that derived from the axial flows. In this sense, it is believed that the far-field conditions do not influence the layer selection.

Suppose that $h \in (h_{circ}, h_{max})$. As $h$ is decreased in this range, the peak value of $\Psi_{-L}(Y)$ decreases and we can expect that the contribution to $D(\boldsymbol{U})$ from $\Omega_{l,1}$ decreases. Essentially, there is less of fluid 1 flowing in and out of $\Omega_{l,1}$ and the region in which fluid 1 can turn around is getting larger. In fluid 2, we suppose that the distortion of the streamlines around the region $\Omega_{l,1}$ as $h$ decreases (see figure 14*a*) does not much affect the contribution to $D(\boldsymbol{U})$ from $\Omega_{l,2}$. Note that there is no contribution to $D(\boldsymbol{U})$ from the static wall layer region and downstream from $\Omega_{l,2}$ the far-field visco-plastic dissipation rate is completely unaffected by any change in $h$.

Now consider what happens for $h < h_{circ}$, when fluid 2 must recirculate. A streamline $\Psi = 0$ enters $\Omega_2$ at $(X, Y) = (L, Y_{L,zero})$. It is notable that $Y_{L,zero} \to Y_{2,Y}$ as $h \to h_{circ}$. Thus, the region of $\Omega_{l,2}$ in which recirculation takes place is initially $O(lY_{2,Y})$. There is a large change in the streamline pattern in $\Omega_{l,2}$ associated with the transition $h \to h_{circ}$. Since always $\tau_{1,Y} < \tau_{2,Y}$ when static layers exist (and typically also $\mu_1 < \mu_2$), we can suppose that the increased contribution to $D(\boldsymbol{U})$ from $\Omega_{l,2}$ at the transition $h \to h_{circ}$ is large, relative to the decrease due to $\Omega_{l,1}$. We therefore suppose that there is a local minimum in $D(\boldsymbol{U})$ very close to $h = h_{circ}$ and that this local minimum is responsible for selecting $h$.

## 6. Summary and discussion

Displacement of visco-plastic fluids in a long slot allows the possibility that completely static layers of the displaced fluid can be left on the walls of the slot after displacement. For symmetric displacements we have shown that the possibility of static layers existing is governed by a single curve relating a critical ratio of the yield stresses to the Bingham number of the displacing fluid $B_1$ (see figure 5). For yield stress ratios $\varphi_Y$ below the critical ratio, the maximum static layer thickness $h_{max}$ depends only on $B_1$ and $\varphi_Y$ for iso-density displacements. For axial displacements with a density difference, a third parameter $\varphi_B$ also controls the maximum layer thickness $h_{max}$. The parameter $\varphi_B$ is a ratio between the buoyancy stress and the yield stress of the displaced fluid. It is interesting to note that although $h_{max}$ is reduced significantly by increasing $\varphi_B$, the critical curve in the $(B_1, \varphi_Y)$-plane denoting $h_{max} = 0$ is not dependent on $\varphi_B$.

Two-dimensional transient displacement computations show also that static residual layers of thickness $h$ exist. Typically static $h$ that are computed from the transient displacements are significantly less than $h_{max}$. Considering a steady-state displacement model, we have shown that static $h$ are predicted remarkably well by the critical layer thickness $h_{circ}$, at which the displaced fluid recirculates. As a practical result, this is possibly the most important contribution of this paper.

We have argued that $h = h_{circ}$ (approximately) locally minimizes the rate of visco-plastic dissipation of kinetic energy. Whilst we believe this explanation to be correct, the explanation is likely only to be valid within parameter ranges where inertia is relatively unimportant.

When $h_{circ} > h_{max}$, static $h$ cannot be predicted by $h_{circ}$, even though $h_{circ}$ is well defined. The computed results in figures 17 and 18 lie close to $h_{circ}$ even when $h_{circ} > h_{max}$. However, this is purely due to the choice of time at which $h$ was computed. At longer times these residual layers decrease, i.e. they are not static. We have not studied this parametric regime extensively. However, in some computations it was observed that $h(t) < h_{max}$ at long times. This is contradictory and not well understood. On the one hand, the displacement front has moved and the axial displacement model should govern interface movement. For this model, we have seen that $h(t) \to h_{max}$ as $t \to \infty$. On the other hand, for thin layers approaching the thickness of a mesh spacing, numerical diffusion will become significant (i.e. for the two-dimensional results, we have no sharp interface). Secondly, as discussed earlier, static layer non-uniformities and consequent coupling with the axial flow seem inherent and will effectively reduce $h_{max}$ in any two-dimensional numerical computation. Finally, it is unclear whether or not the visco-plastic dissipation functional $D(\boldsymbol{U})$ might have other local minima for $h \in (0, h_{max})$ when $h_{circ} > h_{max}$.

The critical layer thickness $h_{circ}$ depends only on the Bingham number of the displacing fluid $B_2$. Using

$$h = \min\{h_{max}, h_{circ}\}$$

as an estimate of static layer thickness appears to be a reasonable engineering rule for iso-density displacements: approximately correct for $h_{circ} < h_{max}$ and a little conservative for $h_{circ} > h_{max}$. The advantage here is that $h = \min\{h_{max}, h_{circ}\}$ depends only on three dimensionless parameters $(\varphi_Y, B_1, B_2)$ and is extremely quick and simple to compute. The computed displacements depend on four dimensionless parameters $(\tau_{1,Y}, \tau_{2,Y}, \mu_1, \mu_2)$, and need sophisticated CFD software.

Transient computations of buoyant displacements have not been presented. The effect of inertia on these displacements also needs to be better understood. From a practical perspective, we have concentrated on flows where inertial effects are believed

to be minimal (except perhaps close to the displacement front). The phenomenon of a static layer is believed to be more acute for slower flows, for which visco-plasticity begins to dominate inertia. For faster flows, it is likely that instabilities arise, either in the parallel flow behind the displacement front or at the front itself. Although these would be of scientific interest to study, from a practical perspective any instabilities are likely to improve the overall displacement and therefore are good. We have focused on the flows that we believe are more likely to result in stable static layers. An in-depth study of both inertia and buoyancy effects is ongoing.

Existence and uniqueness of a solutions to equations (5.1)–(5.5) with the assigned boundary conditions is a non-trivial problem. We tackle this problem in a companion paper (Frigaard, Scherzer & Sona 1999), including the interesting question of which range of values of $h$ can admit solutions.

There are many possible extensions of the work presented here (for example to inclined slots and to Herschel–Bulkley fluid rheologies). The question of convergence of the results towards equivalent results for miscible (and/or) Newtonian fluid displacements also merits attention. Presumably, truly steady-state displacements with a static layer would not be possible in either case. It is interesting to speculate whether the prediction methodology behind $h_{circ}$ can shed light on the problem of selecting the finger width in a miscible Newtonian displacement, i.e. that part of the displacement front that propagates steadily.

We are grateful to the management of Schlumberger for their permission to publish this paper. The work of Giuliano Sona was completed during an internship at Schlumberger Dowell. This internship was partly funded by the European Union through the Leonardo da Vinci Community Programme.

## REFERENCES

Alexandrou, A. N. & Entov, V. 1997 On the steady-state advancement of fingers and bubbles in a Hele-Shaw cell filled by a non-Newtonian fluid. *Eur. J. Appl. Maths* **8**, 73–87.

Barenblatt, G. I., Entov, V. M. & Ryzhik, V. M. 1990 *Theory of Fluid Flows through Natural Rocks*, pp. 44–51, 187–229. Kluwer.

Chen, C.-Y. & Meiburg, E. 1996 Miscible displacements in capillary tubes. Part 2. Numerical simulations. *J. Fluid Mech.* **326**, 57–90.

Cockburn, B. & Shu, C.-W. 1994 Nonlinearly stable compact schemes for shock calculations. *SIAM J. Numer. Anal.* **31**, 607–627.

Comparini, E. 1992 A one-dimensional Bingham flow. *J. Math. Anal. Appl.* **169**, 127–139.

Economides, M. J. 1990 Implications of cementing on well performance. In *Well Cementing* (ed. E. B. Nelson), chap. 1. Schlumberger Educational Services.

Fenie, H. & Frigaard, I. A. 1999 Transient fluid motions in a simplified model for oilfield plug cementing. *Math. Comput. Model.* **30**(7–8), 71–91.

FIDAP, 1998 *FIDAP 8 Theory Manual*, chaps 3–7, 13. Fluent Inc.

Frigaard, I. A. 1998 Stratified exchange flows of two Bingham fluids in an inclined slot. *J. Non-Newtonian Fluid Mech.* **78**, 61–87.

Frigaard, I. A. & Crawshaw, J. 1999 Preventing buoyancy driven flows of two Bingham fluids in a closed pipe; fluid rheology design for oilfield plug cementing. *J. Engng Maths* **36**, 327–348.

Frigaard, I. A. & Scherzer O. 1998 Uniaxial exchange flows of two Bingham fluids in a cylindrical duct. *IMA J. Appl. Maths* **61**, 237–266.

Frigaard, I. A., Howison, S. D. & Sobey, I. J. 1994 On the stability of Poiseuille flow of a Bingham fluid. *J. Fluid Mech.* **263**, 133–150.

Frigaard, I. A. & Scherzer O. 2000 The effects of yield stress variation on uniaxial exchange flows of two Bingham fluids in a pipe. *SIAM J. Appl. Maths* **60**, 1950–1976.

Frigaard, I. A., Scherzer O. & Sona, G. 2000 Uniqueness and non-uniqueness in the steady displacement of two viscoplastic fluids. *Z. Angew. Math. Mech.* in press.

Glowinski R. 1983 *Numerical Methods for Nonlinear Variational Problems*. Springer.

Guillot, D., Hendriks, H., Callet, F. & Vidick, B. 1990 Mud removal. In *Well Cementing* (ed. E. B. Nelson), chap. 5. Schlumberger Educational Services.

Joseph, D. D. & Renardy, Y. Y. 1993 *Fundamentals of Two-Fluid Dynamics. Part II: Lubricated transport, drops and miscible liquids*. Interdisciplinary Applied Mathematics, vol. 4, pp. 324–360. Springer.

Lajeunesse, E. 1999 Déplacement et instabilités de fluides miscibles et immiscibles en cellules de Hele-Shaw. These de l'Universite Pierre et Marie Curie (PhD thesis), Orsay, France.

Lajeunesse, E., Martin, J., Rakotomalala, N. & Salin, D. 1997 3D Instability of miscible displacements in a Hele-Shaw cell. *Phys. Rev. Lett*. **79**, 5254–5257.

Lajeunesse, E., Martin, J., Rakotomalala, N., Salin, D. & Yortsos, Y. 1999 Miscible displacement in a Hele Shaw cell at high rates. *J. Fluid Mech*. **398**, 299–319.

Liu, K. F. & Mei, C. C. 1989 Slow spreading of a sheet of Bingham fluid on an inclined plane. *J. Fluid Mech*. **207**, 505–529.

Liu, K. F. & Mei, C. C. 1994 Roll waves on a layer of muddy fluid flowing down a gentle slope – a Bingham model. *Phys. Fluids* **6**, 2577–2590.

Mineev-Weinstein, M. 1998 Selection of the Saffman-Taylor finger width in the absence of surface tension: an exact result. *Phys. Rev. Lett*. **80**, 2113–2116.

Pascal, H. 1984*a* Rheological behaviour effect of non-Newtonian fluids on dynamic of moving interface in porous media. *Intl J. Engng Sci*. **22**, 227–241.

Pascal, H. 1984*b* Dynamics of moving interface in porous media for power law fluids with a yield stress. *Intl J. Engng Sci*. **22**, 577–590.

Pascal, H. 1986 A theoretical analysis of stability of a moving interface in a porous medium for Bingham displacing fluids and its application in oil displacement mechanism. *Can. J. Chem. Engng* **64**, 375–379.

Petitjeans, P. & Maxworthy, T. 1996 Miscible displacements in capillary tubes. Part 1. Experiments. *J. Fluid Mech*. **326**, 37–56.

Prager, W. 1954 On slow visco-plastic flow. In *Studies in Mathematics and Mechanics*. Volume presented to Richard von Mises. Academic.

Rogerson, A. & Meiburg, E. 1993*a* Shear stabilization of miscible displacement processes in porous media. *Phys. Fluids* A **5**, 1344–1355.

Rogerson, A. & Meiburg, E. 1993*b* Numerical simulation of miscible displacement processes in porous media flows under gravity. *Phys. Fluids* A **5**, 2644–2660.

Saffman, P. G. 1986 Viscous fingering in Hele-Shaw cells. *J. Fluid Mech*. **173**, 73–94.

Saffman, P. G. & Taylor, G. I. 1958 The penetration of a finger into a porous medium in a Hele-Shaw cell containing a more viscous liquid. *Proc. R. Soc. Lond*. A **245**, 312.

Smith, D. K. 1987 *Cementing*. SPE Monograph Series, chap. 6, pp. 82–106. Society of Petroleum Engineers.

Szabo, P. & Hassager, O. 1992 Flow of viscoplastic fluids in eccentric annular geometries. *J. Non-Newtonian Fluid Mech*. **45**, 149–169.

Szabo, P. & Hassager, O. 1997 Displacement of one Newtonian fluid by another: density effects in axial annular flow. *Intl J. Multiphase Flow* **23**, 113–129.

Walton, I. C. & Bittleston, S. H. 1991 The axial flow of a Bingham plastic in a narrow eccentric annulus. *J. Fluid Mech*. **222**, 39–60.

Wilson, S. D. R. 1990 The Saffman-Taylor problem for a non-Newtonian liquid. *J. Fluid Mech*. **220**, 413–425.

Wilson, S. D. R. 1993*a* Squeezing flow of a Bingham material. *J. Non-Newtonian Fluid Mech*. **47**, 211–219.

Wilson, S. D. R. 1993*b* Squeezing flow of a yield stress fluid in a wedge of slowly varying angle. *J. Non-Newtonian Fluid Mech*. **50**, 45–63.

Wilson, S. D. R. & Taylor, A. J. 1996 The channel entry problem for a yield stress fluid. *J. Non-Newtonian Fluid Mech*. **65**, 165–176.

Yang, Z. & Yortsos, Y. C. 1997 Asymptotic solutions of miscible displacements in geometries of large aspect ratio. *Phys. Fluids* **9**, 286–298.

Yortsos, Y. C. & Zeybek, M. 1988 Dispersion driven instability in miscible displacement in porous media. *Phys. Fluids* **31**, 3511–3518.

Zimmerman, W. B. & Homsy, G. M. 1991 Nonlinear viscous fingering in miscible displacement with anisotropic dispersion. *Phys. Fluids* **31**, 3511–3518.